A Mesenchymal Cell Niche in Skin for Acute Myeloid Leukemia

Running title: Extramedullary mesenchymal cell niche in AML

Lakshmi Sandhow[1], Huan Cai[1], Pingnan Xiao[1], Elory Leonard[1], Makoto Kondo[1&], Xiaoyan Sun[2], Anne-Sofie Johansson[1], Karl Tryggvason[3], Maria Kasper[2], Marcus Järås[4], Hong Qian[1*]

[1]Center for Hematology and Regenerative Medicine, Department of Medicine Huddinge, Karolinska Institute, Karolinska University Hospital, SE-141 86 Stockholm, Sweden;

[2]Department of Cell and Molecular Biology, Karolinska Institute, 171 77, Stockholm, Sweden;

[3]Department of Medical Biochemistry and Biophysics, Karolinska Institute, Stockholm, 17177, Sweden;

[4]Department of Clinical Genetics, Lund University, Lund 22184, Sweden.

[&]Current address: Cell Sheet Tissue Engineering Center (CSTEC), Department of Pharmaceutics and Pharmaceutical Chemistry, Health Sciences, University of Utah, 30 South 2000 East, Salt Lake City, Utah 84112, USA.

***Corresponding author:** Hong Qian, hong.qian@ki.se

Text word count: 3993 excluding acknowledgments

Abstract word count: 149

Figures: 7 main figures, 6 supplemental figures

References: 61

Key points:

- Leukemic cells infiltrated in skin are capable to generate AML post-transplantation
- Mesenchymal progenitors in skin contribute to forming the niche for AML cells
- Skin mesenchymal progenitors protect AML stem cells possibly by mitochondrial transfer
- *Lama4* deletion in skin mesenchymal niche promotes AML cell proliferation and chemoresistance to cytarabine

Abstract (149)

Leukemia cutis or leukemic cell infiltration in skin is one of the common extramedullary manifestations of acute myeloid leukemia (AML) and signifies a poorer prognosis. However, its pathogenesis and maintenance remain understudied. Here, we report massive AML cell infiltration in mouse skin. These cells were retained in the skin post-chemotherapy and could regenerate AML post-transplantation. The niche characterization revealed that skin harbored mesenchymal progenitor cells (MPCs) with a similar phenotype as BM mesenchymal stem cells. These skin MPCs maintained and protected AML-initiating stem cells (LSCs) from chemotherapy *in vitro* possibly via mitochondrial transfer. Furthermore, *Lama4* deletion in skin MPCs promoted AML LSC proliferation and chemoresistance. Importantly, more chemoresistant AML LSCs were retained in *Lama4*$^{-/-}$ mouse skin post-cytarabine treatment. Our study reveals the characteristics and previously unrecognized roles of skin mesenchymal niches in maintaining AML LSCs and protecting them during chemotherapy, meriting future exploration of their impact on AML relapse.

Key words: Early B-cell Factor 2, skin, mesenchymal progenitor cells, acute myeloid leukemia, hematopoietic stem cells, stem cell niche, leukemic stem cells, drug resistance, cytarabine, bone marrow

Introduction

Leukemia cutis (leukemic cell infiltration in skin) is one of the commonly observed extramedullary manifestations in acute myeloid leukemia (AML).[1,2] It is associated with poor survival in patients with AML.[2-4] However, our understanding of its pathogenesis is very limited. This has been mainly due to lack of knowledge about the extramedullary niches where AML cells infiltrate and are maintained.

For decades, great efforts have been put to elucidate the contribution of the hematopoietic niche in bone marrow (BM) to normal and malignant hematopoiesis. The BM niche consists of various types of cells including mesenchymal stem cells (MSCs), mesenchymal progenitors (MPCs), osteoblasts and endothelial cells. Accumulating evidence has shown that BM MSCs and MPCs play important roles in maintaining normal hematopoiesis and in the development of myeloid malignancies including AML.[5,6] Molecular alterations in these niches could lead to malignant transformation of hematopoietic cells.[7-9] During leukemia development, the leukemic cells can alter the BM niches, which renders the niche to become favorable for

leukemic cell growth but harmful for normal hematopoiesis.[6,10-13] Using a *Cre-LoxP* mouse model allowing for selective deletion of the MSC population, we have shown that loss of MSCs accelerates AML progression.[6,10] However, these markers are not unique for the mesenchymal cells in BM, thus, it is not clear whether the mesenchymal cell niches in extramedullary organs like skin are also affected, thereby contributing to the AML progression.

Besides BM, extramedullary organs such as adipose tissue have been reported to accommodate hematopoietic stem and progenitor cells (HSPCs) in the stromal vascular fraction.[14] In blast crisis of chronic myeloid leukemia, the gonadal white adipose tissue is infiltrated by leukemic cells that adapt to the extramedullary niche and transform into resistant leukemia-initiating stem cells (LSCs) marked by CD36 expression.[15] These findings indicate that extramedullary organs may serve as niches for HSPCs and LSCs.

Existing evidence suggests that skin might contain an MSC-like cell population.[16-19] However, their biological properties and contribution to hematopoiesis and leukemia remain unexplored. Knowledge of this would be essential for understanding the pathology of extramedullary leukemia in the skin, and would thus provide new insights into identifying new potential therapeutic targets that may be translated into new treatment strategies for AML patients with leukemia cutis.

We here in a transplantation-induced AML mouse model detected massive infiltration of AML cells in the skin. Importantly, these skin AML cells from mice at steady-state or post-chemotherapy could regenerate AML post-secondary transplantation. Characterization of the AML niche revealed the molecular features and developmental hierarchy of the skin MPCs. The MPCs expressing Early B-cell Factor 2 (Ebf2) contribute to mesenchymal cell turnover in the skin and were reduced post-AML onset. The skin MPCs could maintain and protect AML LSCs and loss of Lama4 in skin MPCs promoted AML cell maintenance and resistance to chemotherapy. Altogether, our study revealed the characteristics and a previously unrecognized role of skin MPCs in maintaining AML LSCs during AML development and chemotherapy.

Results

The AML cells infiltrated in skin can regenerate AML post-transplantation

We have here studied extramedullary leukemia in skin by using an MLL-AF9^{+} AML cell transplantation-induced AML mouse model (**Figure 1A**). Post-symptomatic AML onset, we detected the massive infiltration of the AML cells in the dorsal skin by fluorescence-activated

98 cell sorting (FACS) (**Figure 1B-1D**). The frequency was higher (41% of skin CD45$^+$ cells)
99 than that in the blood, but lower than that in BM (>95%) (**Figure 1B-1C**). Confocal imaging
100 showed that these AML cells mainly resided at perivascular sites in the skin (**Figure 1D**).
101 It is not known whether the AML cells infiltrated in skin contain LSCs capable to regenerate
102 leukemia, particularly after chemotherapy. We therefore sorted the AML cells from the mouse
103 skin post-cytarabine (Ara-C) or vehicle treatment and transplanted them into secondary
104 recipients without prior irradiation (**Figure 1E-1K**). Notably, these AML cells even in a low
105 dose (1000 cells/mouse) rapidly and efficiently generated AML in the recipients without pre-
106 conditioning, as indicated by short survival (**Figure 1F**), low platelet counts (**Figure 1G**), high
107 AML engraftment in the BM (**Figure 1H-1I)** and splenomegaly (**Figure 1J**). These results
108 demonstrate the leukemia-initiating capacity of the AML cells residing in the skin tissue not
109 only under steady-state but also after chemotherapy, indicating their potential impact in AML
110 relapse.
111
112 **Skin harbors Ebf2$^+$ and Ebf2$^-$ MPC subsets with similar immunophenotype to BM MSCs**
113 To understand how the leukemic cells were maintained in the skin tissue, we explored the
114 role of the extramedullary microenvironment in the skin using a similar approach as was used
115 for characterizing the BM niche. BM MSCs have been shown to be involved in AML
116 progression in mice[6]. They are defined by a phenotype of lacking expression of CD44,
117 hematopoietic (CD45/TER119) and endothelial (CD31) cell markers, but positive for
118 PDGFRa/CD140a, SCA1 and CD51.[6,9,11,20,21] The primitive MSCs in mouse BM can be
119 identified by Ebf2 expression[22] and can generate MSCs that lack Ebf2.[6] However, the
120 phenotype of native skin MSCs remains unknown. The question is whether the cells with
121 similar features exist in skin and play a role in the AML cell maintenance under steady-state
122 and following chemotherapy. To answer this, we first characterized mesenchymal stem and
123 progenitors in the skin by using the *Ebf2-Egfp* reporter mice. Similar to BM, a fraction of
124 CD45$^-$TER119$^-$CD31$^-$ skin stromal cells expressed Ebf2 (**Figure 2A**). The Ebf2$^+$ cells
125 accounted for about 2% and 5% of total live cells and CD45$^-$TER119$^-$CD31$^-$ stromal cells,
126 respectively (**Figure 2B-2C**). Phenotypically, skin Ebf2$^+$ cells highly expressed
127 PDGFRa/CD140a and SCA1 (PαS) whereas about 41% of the Ebf2$^-$ cells were PαS cells
128 (**Figure 2D**).
129 Functionally, both the Ebf2$^+$ and Ebf2$^-$ cells contained CFU-Fs, a colony-forming unit
130 characteristic for MSCs (**Figure 2E, Figure S1A**). The CFU-Fs in the Ebf2$^+$ cells were

131 generated exclusively by the SCA1$^+$ population (**Figure 2F**). Both Ebf2$^+$ and Ebf2$^-$PαS cell
132 populations showed similar proliferation kinetics after passage 5-6 (**Figure S1B**) and were able
133 to differentiate towards osteogenic and adipogenic lineages *in vitro* (**Figure S1C**). However,
134 they failed to differentiate into chondrocytes in either monolayer or micromass pellet culture
135 in which condition BM MSCs could differentiate into chondrocytes (**Figure S1C-S1D**). These
136 data indicate that the Ebf2$^+$ and Ebf2$^-$PαS cells in mouse skin may represent bipotential MPCs
137 although they have the same immunophenotype as BM MSCs.
138
139 **Single-cell assay confirms osteo-adipo bipotentials of skin Ebf2$^+$ and Ebf2$^-$PαS cells**
140 To validate the identity of the skin stromal subsets, we characterized these cells at single
141 cell level. Limiting dilution experiment revealed that the CFU-F frequency in both skin Ebf2$^+$
142 and Ebf2$^-$PαS fractions was as high as 1 in 4 (**Figure 2G, 2I**). Of 8 randomly selected CFU-
143 Fs from single Ebf2$^+$ cells, 7 (88%) showed both osteogenic and adipogenic differentiation
144 potency although to different degrees (**Figure 2H, 2K**). However, only 43% (3 clones of 7) of
145 the Ebf2$^-$PαS cells showed bi-lineage potency toward osteoblasts and adipocytes (**Figure 2J-**
146 **2K**). The chondrogenic potency, however, was not evaluated at single cell level since none of
147 these cell subsets differentiated into chondrocytes at the bulk level. The self-renewal capacity
148 of the Ebf2$^+$ and Ebf2$^-$ cells was evaluated by serially replating of single CFU-F derived from
149 the single sorted cells. Three out of 5 clones from 12 CFU-Fs initially generated by single
150 Ebf2$^+$ cells could be serially replated for beyond 10 passages while the other 2 clones were
151 able to expand to passage 5 (**Figure 2L**). Meanwhile, only 1 in 3 CFU-F clones derived from
152 9 Ebf2$^-$PαS cells-derived CFU-Fs could be serially replated for over 8 passages (**Figure 2L**),
153 indicating a limited self-renewal capacity of the Ebf2$^-$PαS cells. These data further support the
154 notion that the skin Ebf2$^+$ and Ebf2$^-$PαS cells are enriched with osteo-adipogenic MPCs.
155
156 **Skin Ebf2$^+$ cells are mainly located at perivascular sites**
157 Similar to that in mouse BM, the skin Ebf2$^+$ cells did not express endothelial cell marker CD31
158 (**Figure S2A**). However, the Ebf2$^+$ cells highly expressed PDGFRb/CD140b, a marker
159 expressed in pericytes[23] and niche-forming perivascular cells in BM[24] (**Figure S2B**), pointing
160 to a pericyte phenotype. Confocal imaging illustrated that the majority of the Ebf2$^+$ cells were
161 adjacent to the endothelial cells in the skin (**Figure 3A-3B**, **Figure S2C**). Some scattered Ebf2$^+$
162 cells were also found in dermal panniculus carnosus, a layer of striated muscle (**Figure 3A**).
163 Approximately 55% and 41% of the Ebf2$^+$ cells were positive for the pericyte marker NG2,

164 respectively (**Figure S2D, S2F**), and 81% of them expressed α-smooth muscle actin (SMA)
165 (**Figure S2E-S2F**), reported to mark pericytes in BM[25]. Altogether, these data suggest a
166 perivascular origin and heterogeneity of the skin Ebf2$^+$ cells.
167
168 **The Ebf2$^+$ cells in skin contribute to the mesenchymal cell turnover**
169 To understand how mesenchymal cell niche in the skin is maintained, we determined the
170 physiological contribution of the Ebf2$^+$ stromal cells to the niche formation by lineage-tracing
171 using Tg*Ebf2-Egfp xCre^{ERT2}* X *Rosa26-tomato* mice (**Figure 3C**). This mouse model allowed
172 us to track the fates of the Ebf2$^+$ cells *in vivo* since the Ebf2$^+$ cells express GFP and their
173 progeny is marked by Tomato after tamoxifen (TAM) injection. About 15% of total Ebf2$^+$ cells
174 were Tomato$^+$(Ebf2$^+$Tomato$^+$) cells at 3 months after TAM induction (**Figure S3A-S3B**). The
175 Ebf2$^+$Tomato$^+$ cells could generate Ebf2$^-$PαS MPCs and more mature CD45$^-$TER119$^-$CD31$^-$
176 CD44$^-$CD140a$^+$SCA1$^-$ stromal cells (**Figure 3D-3E**), indicating the important role of the Ebf2$^+$
177 cells in maintaining the mesenchymal cell compartment in the skin.
178 The fraction of the Ebf2$^+$Tomato$^+$ cells within stromal cells remained constant up to 12
179 months post TAM induction (**Figure 3E**), which is likely attributed to their self-renewal ability.
180 However, the Ebf2$^-$Tomato$^+$ cells which were produced by the Ebf2$^+$Tomato$^+$ cells increased
181 from 11% at 3 months to 21% at 6 months post-TAM injection, then remained stable at 12
182 months (**Figure 3E**). Within the newly generated Ebf2$^-$Tomato$^+$ cells, the majority were PαS
183 MPCs and about 5% were the CD140a$^+$SCA1$^-$ cells (**Figure 3F**). Within the total PαS MPCs,
184 only about 0.5% were Ebf2$^+$Tomato$^+$ cells and 30% were the newly generated Ebf2$^-$Tomato$^+$)
185 PαS cells at 6 months post-TAM (**Figure S3C-S3E**). These data suggest a substantial
186 contribution of the Ebf2$^+$ MPCs to generating the Ebf2$^-$Tomato$^+$PαS MPCs while maintaining
187 the Ebf2$^+$ cell pool. The actual contribution might have been underestimated due to the
188 incomplete *Cre* activation in the Ebf2$^+$ cells, reflected in the presence of Ebf2$^+$Tomato$^-$ cells
189 shortly (2-3days) after TAM injection (data now shown).
190 Similar to the Ebf2$^+$ cells, the Ebf2$^-$Tomato$^+$ cells were mainly distributed in the lower
191 dermis and adjacent to CD31$^+$ endothelial cells (**Figure 3G**). Unlike the Ebf2$^+$ cells, the Ebf2$^-$
192 Tomato$^+$ cells lacked NG2 expression (**Figure S3F**). Only 19% and 28% of the Ebf2$^-$Tomato$^+$
193 cells expressed NESTIN and α-SMA, respectively (**Figure S3G-SI**),
194 Altogether, skin harbors Ebf2$^+$ and Ebf2$^-$PαS MPCs with a similar phenotype as BM MSCs.
195 The Ebf2$^+$ MPCs reside at the top of the developmental hierarchy and contribute to
196 mesenchymal cell generation in the skin.

197

198 **Skin MPCs play a role in maintaining normal hematopoietic and AML cells *in vitro***

199 Identification of the skin MPC populations made it possible to analyze their potential role
200 in the maintenance of AML cells. We first evaluated the function of skin MPC subsets in
201 supporting normal hematopoietic stem cells (HSCs) in a co-culture system and compared to
202 BM MSCs (**Figure S4A**). Similar to their BM counterparts, both skin Ebf2$^+$ and Ebf2$^-$PαS
203 MPCs were able to maintain HSC activities**,** indicated by similar numbers of CFU-Cs generated
204 from the SCA1$^+$KIT$^+$(LSK)CD150$^+$ cells after the co-coculture with skin MPCs or BM MSCs
205 (**Figure S4B-S4C**). This finding was further supported by the similar cobblestone area forming
206 cells (CAFCs) generated from the BM LSK cells co-cultured with the skin MPCs or BM MSCs
207 (**Figure S4D-S4E**). The BM Ebf2$^-$PαS cells displayed better capacity in supporting CAFC
208 formation from the LSK cells than the BM Ebf2$^+$ MSCs (**Figure S4F**). Altogether, these data
209 indicated that skin MPCs possessed similar hematopoiesis supportive function as BM MSCs.

210 To assess the role of skin MPCs in supporting AML LSC growth, we next performed CAFC
211 assay of MLL-AF9$^+$ AML cells (**Figure 4A**). Like BM Ebf2$^+$ MSCs, skin MPC subsets could
212 support CAFC formation from the AML cells, but to a lesser degree than the BM Ebf2$^-$PαS
213 cells (**Figure 4B-4C**).

214 Increasing evidence suggests that BM stromal cells may protect leukemia cells from
215 cytostatic drugs.[26-30] However, it is not known if extramedullary stromal cells have similar
216 functions. We then tested the chemoprotective function of skin MPCs by CAFC assay. We
217 administered Ara-C 2 days after seeding the MLL-AF9$^+$ AML cells to the MPCs to allow for
218 efficient cell-cell interactions (**Figure 4A**). Both skin Ebf2$^+$ and Ebf2$^-$PαS cells could protect
219 the AML LSCs from Ara-C treatment, demonstrated by the persistence of residual CAFCs after
220 Ara-C treatment, in striking contrast to the efficient killing of the AML cells cultured alone
221 (**Figure 4D-4E**). No difference in the frequency of KIT$^+$ AML cells, representing AML
222 LSCs,[31] was observed among all the co-cultures (**Figure 4F**). However, the numbers of the
223 residual KIT$^+$ LSCs were significantly increased in the co-cultures with the stromal cells
224 compared to the monoculture post-Ara-C treatment (**Figure 4G**). CD36 was reported to be a
225 marker for chemoresistant leukemic cells.[15,32,33] Post-Ara-C, the CD36$^+$ AML cells were
226 selectively enriched in all the co-cultures except that with skin Ebf2$^-$PαS MPCs (**Figure 4H**),
227 however, only in the culture with skin MPC subsets, significant more CD36$^+$ AML cells were
228 retained (**Figure 4I**). These data indicate a previously unrecognized role of skin MPCs in AML
229 LSC maintenance and protection.

230

231 **The altered mesenchymal niches in the skin during AML development.**

232 Niche-remodeling in BM has been considered as one of the mechanisms contributing to
233 leukemia progression[6,34-36]. By confocal imaging, we observed the perivascular location of the
234 AML cells (**Figure 1D**) and the localization adjacent to the skin Ebf2/GFP$^+$ MPCs in the skin
235 (**Figure 4J**). We then evaluated whether the skin cellular niches were remodeled by the AML
236 cells as observed in their BM counterparts.[6] The proportion of Ebf2$^+$ MPCs in the skin stromal
237 cells were reduced post-symptomatic onset of AML (**Figure 4K-4L**) whereas the Ebf2$^-$PαS
238 cells remained unchanged (**Figure 4M-4N**). This finding is consistent with the reduced PαS
239 cell fraction in the Ebf2$^+$ cells in AML mouse BM and might contribute to further AML cell
240 proliferation since deletion of Ebf2$^+$ cells in mice led to AML acceleration.[6] In addition, while
241 the total CD31$^+$ endothelial cells were unaltered, however, as observed in BM,[6] the
242 CD31$^+$SCA1$^+$ arteriolar endothelial cells were significantly increased (**Figure 4O-4P**),
243 indicating an increase of arterioles in dorsal skin during AML development.

244

245 **Molecular evidence for the role of skin MPCs in hematopoiesis and AML**

246 To investigate the molecular mechanisms behind the hematopoiesis-supportive function of
247 the skin MPCs, we performed RNA sequencing on the freshly sorted skin Ebf2$^+$ and Ebf2$^-$PαS
248 MPCs. This revealed a distinct transcriptional profile of skin MPCs and BM MSCs with 1150
249 and 816 genes differentially expressed between skin Ebf2$^+$ and Ebf2$^-$PαS MPCs compared to
250 BM MSCs, respectively (**Figure 5A**). However, only 135 genes were differentially expressed
251 between the skin Ebf2$^+$ and Ebf2$^-$PαS cells. Among them, the genes associated with TNFα
252 signaling, angiogenesis and epithelial to mesenchymal transition, such as *Lama5* and *Tnc*, were
253 upregulated while the cell proliferation genes were downregulated in the more primitive Ebf2$^+$
254 cells (**Figure 5B, Figure S5A**). We then compared skin MPC pool (Ebf2$^+$ and Ebf2$^-$PαS) with
255 BM MSCs. The genes related to skin tissue maintenance (*Krt14*, *Krt19*) and adipogenesis
256 (*Fabp4*) were upregulated in the skin MPCs (**Figure 5C**), showing tissue origin-related
257 characteristics of these cells. Consistent with the limited chondrogenic differentiation capacity
258 of skin MPCs (**Figure S1C-S1D**), the genes associated with osteogenesis and chondrogenesis
259 were downregulated in the cells (**Figure S5B**). Conversely, skin MPCs were enriched with
260 genes related to fatty acid metabolism and oxidative phosphorylation indicating a distinct
261 metabolic profile between the skin and BM MSCs (**Figure 5D-5E**). Furthermore, the genes

262 related to inflammatory response were enriched in the skin MPCs relative to BM MSCs
263 (**Figure 5E-5F, Figure S5C**), indicating a possible pro-inflammatory phenotype of skin MPCs.
264
265 Notably, no overall significant difference in the hematopoiesis supportive gene expression
266 between the skin MPCs and BM MSCs (**Figure 5G**). The findings were confirmed by Q-PCR
267 of the genes in these freshly sorted cells (**Figure 5H**). Similar to BM MSCs, both skin MPC
268 subsets expressed *Cxcl12*, *Kitl* (*Scf*), *Jag1, Lama4* and *Angptl1,* all of which are known to be
269 critical for hematopoiesis maintenance and regeneration.[37-44] The expressions of *Kitl*, *Jag1* and
270 *Lama4* were even significantly higher in skin Ebf2^{+} and Ebf2^{-}PαS cells than that in BM MSCs.
271 Moreover, the expression of *Spp1,* a negative regulator of HSC expansion,[45] was lower in skin
272 MPCs than that in BM MSCs (**Figure 5C, 5H**).This finding support the similar function of
273 skin MPCs and BM MSCs for HSCs and AML LSCs.
274
275 **Enhanced mitochondrial transfer from skin MPCs to AML cells contributed to the**
276 **chemoprotection of AML cells**
277 To reveal the mechanisms underlying the function of skin MPCs in maintaining and
278 protecting AML LSCs, we examined the metabolic support from skin MPCs to AML cells in
279 coculture since the genes related to oxidative phosphorylation and fatty acid metabolism are
280 enriched in the skin MPCs. Mitochondria transfer has been reported as one of the protective
281 mechanisms during chemotherapy in leukemias to provide energy support and anti-oxidant
282 machinery leading to modulating oxidative stress indued by chemotherapy[35,46-48]. In a co-
283 culture with mitochondria-prelabeled skin MPCs (**Figure 6A**), we detected enhanced
284 mitochondrial transfer from skin MPCs to the AML cells compared to BM MSCs (**Figure 6B-**
285 **6C**). Correspondingly, the AML cells cocultured with skin MPCs showed lower ROS levels
286 and higher viability during Ara-C treatment (**Figure 6D-6E**). These data indicated that skin
287 MPCs could maintain AML LSCs and protect them from Ara-C treatment *in vitro* possibly by
288 reducing oxidative stress. Thus, skin MPCs could be an important element in creating an
289 extramedullary sanctuary for AML LSCs.

290 ***Lama4* loss in skin MPCs enhanced AML LSC proliferation and chemoprotection *in vitro***
291 *Lama4* was highly expressed in skin MPCs (**Figure 5H**) and we have found that *Lama4* loss
292 in mice promoted AML LSC proliferation, chemoresistance, and relapse.[35] This has tempted
293 us to test the impact of *Lama4* deletion in skin MPCs on AML LSC growth (**Figure 6F**). We
294 observed increased AML cell proliferation and chemoresistance to Ara-C at 24h post-the co-

295 culture *Lama4*$^{-/-}$ skin MPCs (**Figure 6G**). Further CAFC assay indicated that *Lama4*$^{-/-}$ skin
296 MPCs promoted AML LSC proliferation and chemoresistance to Ara-C (**Figure 6H**),
297 suggesting a suppressive impact of *Lama4* expression in skin MPCs on AML cell growth and
298 chemoresistance.
299
300 **The increased chemoresistant AML cells in *Lama4*$^{-/-}$ mouse skin post-Ara-C treatment**
301 To further explore the molecular mechanism involving in the role of the extramedullary niche
302 in the skin for maintaining residual AML cells after chemotherapy, we here took advantage of
303 *Lama4*$^{-/-}$ mice (**Figure 7A**) where AML progression and relapse are accelerated.[35] There was
304 no homing preference of the AML cells to *Lama4*$^{-/-}$ skin and BM (**Figure S6**). One day post-
305 Ara-C treatment, confocal imaging illustrated more residual AML cells retained in *Lama4*$^{-/-}$
306 mouse skin, compared to that in *Lama4*$^{+/+}$ mice following Ara-C treatment (**Figure 7B**).
307 However, such a difference was not detected by FACS analysis while the elimination of the
308 AML cells from the PB and skin were clearly observed (**Figure 7C**). It is possible that some
309 of the remaining AML cells were lost during enzymatic digestion of the skin for FACS whereas
310 confocal imaging was performed on the tissue fixed directly after dissecting. It is important to
311 note that the chemoresistant CD36^{+} AML cells[15,33], not KIT^{+} cells were enriched in *Lama4*$^{-/-}$
312 mouse skin post-Ara-C treatment (**Figure 7D**), which was not observed in the BM, as
313 reported.[35] These data suggest that *Lama4* expression in skin mesenchymal niche play a role in
314 maintaining the chemosensitivity of AML cells in the skin to Ara-C.
315
316 **Discussion**

317 We here report that skin tissue harbored two distinct MPC subsets, the Ebf2^{+} and Ebf2^{-}PαS
318 cells, sharing a similar phenotype with BM MSCs.[20,49,50] During AML development, similar to
319 leukemia cutis observed in patients, a substantial amount of AML cells infiltrated in mouse
320 skin. The AML cells were distributed along vascular sites and co-localized with the skin Ebf2^{+}
321 cells. Importantly, these AML cells isolated from mice at steady-state and after chemotherapy
322 could initiate AML post-transplantation into immunocompetent mice. Molecular
323 characterization of the skin MPCs showed high expression of *Lama4*, *KitL* and *Jag1*, known
324 to be important for normal hematopoiesis maintenance and leukemic cell proliferation.[31,35,37-
325 44,51] The skin mesenchymal cell niche maintained AML LSCs and protected them from
326 chemotherapeutic agent Ara-C. Furthermore, Lama4 loss in skin MPCs promoted AML
327 proliferation and chemoresistance. Our study provides evidence for the characteristics and

328 previously unrecognized role of skin mesenchymal cell niche during AML development and
329 after chemotherapy.
330
331 Leukemia cutis is commonly observed in monocytic AML (FAB, M5) and pediatric patients
332 with congenital leukemia are prone to develop leukemia cutis, ranging from 25% to 30% of
333 the cases.[52] It also correlates with manifestations of other extramedullary sites and is associated
334 with a poor prognosis in patients.[1-3] However, leukemia cutis has been understudied. Its impact
335 on AML relapse remains unexplored. We here show AML-regenerating capacity of the residual
336 AML cells in skin post-chemotherapy, pointing to a possible involvement of these leukemic
337 cells in the relapse of AML. In patients, leukemia cutis is usually present concurrently with
338 AML cell infiltration in BM. However, in some cases, it may precede systemic involvement,[4]
339 and it is unclear whether the leukemic cells infiltrated in the skin originate from BM.
340
341 We here for the first time show the chemoprotective role of skin MPCs for AML LSCs.
342 Multiple mechanisms might be involved in the protection. Mitochondrial transfer from stromal
343 cells to leukemic cells has been reported to be one of the mechanisms to protect leukemic cells
344 to survive from chemotherapy by providing antioxidant system to counteract the therapy
345 induced oxidative stress.[53] We here detected a mitochondrial transfer from skin MPCs to the
346 AML cells during chemotherapy *in vitro,* even in a greater degree, than that from BM MSCs.
347 This finding is in line with the enrichment of oxidative phosphorylation genes in skin MPCs.
348 In addition, *Lama4* expression in skin MPCs seemed to maintain AML LSC chemosensitivity
349 since *Lama4* loss in skin MPCs led to enhanced proliferation and chemoprotection of AML
350 LSCs. In line with this, the residual chemoresistant $CD36^+$ AML cells in *Lama4*$^{-/-}$ skin were
351 increased post-Ara-C treatment. Such an effect was not observed in the BM. One possible
352 reason could be the differential expression *of Kitl*, *Jag1* and *Lama4*, known to be important for
353 AML development.[31,35,54] Furthermore, the upregulated inflammatory genes in skin MPCs
354 might have contributed to this effect.
355 Our findings of the identity and immunophenotype of skin MPCs will facilitate the
356 prospective isolation of the cells for further characterization *ex vivo*. The skin $Ebf2^+$ MPCs co-
357 express pericyte markers like CD140b/PDGFRb, NG2 and α-SMA and their perivascular
358 location indicated their pericyte phenotype. A contribution of skin $Ebf2^+$ cells to mesenchymal
359 cell turnover was illustrated by the *in vivo* lineage-tracing. The adjacent localization of the
360 $Ebf2^+$ cells to the AML cells in skin indicated a possibility that these cells might act as a niche

361 component for maintaining AML cells. This notion was supported by another important finding
362 showing a supportive function of skin MPCs for AML LSCs. The fractions skin Ebf2^{+} MPCs
363 were reduced after symptomatic AML onset, leading to a reconstructed niche, which might in
364 turn further promote AML progression since Ebf2^{+} cell deletion in mice accelerated AML
365 development, as reported.[6]

366 In summary, we here report that skin harbors primitive Ebf2^{+} MPCs and the downstream
367 Ebf2^{-} MPCs. These MPCs are colocalized with AML cells at perivascular sites during AML
368 development. The residual AML cells in the skin after chemotherapy can regenerate leukemia
369 post-transplantation, indicating the existence of AML LSCs in the skin. The skin MPCs can
370 provide metabolic support for AML cells to protect them from chemotherapy *in vitro*. Loss of
371 *Lama4* in skin MPCs further enhances their supportive and chemoprotective function for the
372 leukemic cells. We for the first time provide evidence for the roles of skin mesenchymal cell
373 niche for AML LSC growth and chemotherapy response, as well as the impact of *Lama4*
374 expression on the niche protection or support. These findings warrant future studies on the role
375 of skin mesenchymal niches in chemotherapy response and relapse of AML patients.
376

377 **Methods**

378 **Mice**

379 *Ebf2-Egfp* reporter FVB/N mice[22] at 8 to 14-week old were used. Transgenic *Ebf2-Egfp*X*Ebf2-*
380 *Cre^{ERT2}*X *Rosa26^{loxp}Stop^{loxp}-Tomato* mice were generated by crossing *Ebf2-Egfp* with *Ebf2-*
381 *Cre^{ERT2}*X*Rosa26^{loxp}Stop^{loxp}-Tomato* mice for lineage tracing. To activate Cre, tamoxifen (TAM)
382 (Sigma) was intraperitoneally injected at 3mg/20g body weight for 3 times every second day.[6]
383 *Lama4$^{-/-}$* C57BL/6 mice were generated as described.[55] All mice were maintained in specific-
384 pathogen-free conditions in the animal facility of Karolinska Institute. Animal procedures were
385 approved by local ethics committee (ethical number 1869) at Karolinska Institute (Stockholm,
386 Sweden).
387

388 ***In vivo* lineage tracing**

389 This was performed as previously described.[6] Dorsal skin from triple transgenic *Ebf2-Egfp* x
390 *Ebf2-Cre^{ERT2}* x *Rosa26^{loxp}Stop^{loxp}- Tomato* mice[6] were collected at 3, 6 and 12 months after
391 tamoxifen injection. Approximately, 1x1cm of dorsal skin tissue was fixed and embedded in
392 OCT for whole mount immunofluorescence. For evaluating the frequency of Ebf2^{+} cells and
393 their progeny (Tomato^{+}), 2 x 2cm of dorsal skin tissue was processed for skin MPC isolation

394 by fluorescence-activated cell sorting (FACS) (BD FACS Aria^{TM} III). For defining the gates
395 for GFP^{+} and Tomato^{+} cells, cells from bi-transgenic or single transgenic mouse were used as
396 fluorescence-minus one (FMO) controls. After excluding dead cells by propidium iodide (PI)
397 staining, the CD45^{-}TER119^{-}CD31^{-} stromal cells were gated. Subsequently, the CD44^{-} fractions
398 were divided based on CD140a and SCA1 expression.
399
400 **Ara-C treatment and detection of residual AML cells *in vivo*** was performed as described
401 in the related study[35] .

402 **Skin MPC isolation by FACS**
403 Mouse dorsal skin was minced and digested with 0.2% collagenase II (CLSII Worthington
404 Biochemicals) in PBS supplemented with 20% FBS for 60 minutes at 37°C. After washing
405 with PBS/20%FBS followed by PBS, the digested skin tissue was treated with 0.05% trypsin-
406 EDTA (GIBCO) for 10 to 15minutes at 37°C. Cell suspension was spun down at 300g for
407 10minutes. Mononuclear cells were then blocked with FcR (CD16/32) antibody and stained
408 with CD45, TER119, CD31, CD44, CD140a, and SCA1 for 15minutes at 2-8°C. Dead cells
409 were excluded by propidium iodide (PI) staining. For sorting native skin MPCs, hematopoietic
410 and endothelial populations were firstly excluded (CD45^{-}TER119^{-}CD31^{-}) and Ebf2 gate was
411 then defined based on Fluorescence Minus One (FMO) using skin mononuclear cells from a
412 non-transgenic mouse. Skin Ebf2^{+} and Ebf2^{-} cells were sorted on a FACS Aria III Sorp (BD
413 Biosciences, San Jose). See Table S1 for detailed antibody information.

414 **Generation of MLL-AF9-induced AML mouse model**
415 AML mouse model was induced as previously described.[6] Briefly, 250.000 MLL-AF9
416 expressing cells were intravenously injected into non-irradiated mice to generate the AML
417 mouse model. For detecting AML infiltration in dorsal skin tissue, 1x10^{6} of MLL-AF9
418 previously generated in DsRed C57BL/6J transgenic mice[56] were intravenously injected into
419 sublethally irradiated (6Gy) *Lama4*$^{+/+}$ and *Lama4*$^{-/-}$ mice, as described[35]. At day 15, the mice
420 were treated intraperitoneally with Cytarabine (Ara-C, Jena Bioscience) at the dose of
421 700mg/kg body weight, daily for 5 consecutive days. The mice were sacrificed one day after
422 the last injection for AML engraftment analysis in peripheral blood (PB), BM and dorsal skin
423 by FACS. The distribution of residual AML cells in dorsal skin was visualized by confocal
424 imaging.
425

426 **Serial transplantation**

427 To test the leukemia-initiating capacity of the AML cells infiltrated in skin tissue, the AML
428 CD45.1^{+} cells were sorted from skin tissue of the mice that have developed AML post-AML
429 cell injection. The mice were treated with normal saline or Ara-C for 5 days at day 20-21 after
430 AML cell injection. The AML cells in skin were collected 2-3days after the last injection,
431 sorted by FACS and transplanted into non-irradiated secondary C57BL/6J recipient mice via
432 tail vein at a dose of 1000 or 5000 cells per mouse. The AML development was monitored by
433 blood analysis using FACS and Sysmex as well as by assessing the general health conditions.
434 The survival rate of the mice was estimated based on the date when the mice were found dead
435 or in moribund status. Bones and blood were collected for determining AML engraftment.
436

437 **Multilineage differentiation assay**

438 This was done as described [6]. The skin Ebf2^{+}, Ebf2^{-} and Ebf2^{-}PαS cells were expanded in
439 culture and plated at 400cells / cm^{2} to each well of 24-well plate. For osteogenic differentiation,
440 cells were cultured with complete osteogenic medium mixed by human/mouse StemXVivo
441 osteogenic / adipogenic base medium (CCM007, R&D Systems) and mouse StemXVivo
442 ostegenic supplement (CCM009; R&D Systems) under normoxic condition for 14-21 days.
443 Differentiation toward osteoblast was evaluated by 1% alizarin red S (Catalog no A5533,
444 Sigma) staining after cell fixation with cold methanol. For adipogenic differentiation, the
445 culture was performed with DMEM containing 10% FBS, 10mM HEPES (1M), 100U of
446 penicillin/streptomycin, 10^{-4} M 2-Mercaptoethanol (Sigma, catalog no.M7522), 5μg/mL
447 insulin (Catalog no I6634, Sigma), 20μM Indomethacin (Catalog no I7378, Sigma), 0.0115
448 mg/mL isobutylmethylxanthine (Catalog no I-7018, Sigma), and 10^{-6} M dexamethasone
449 (Catalog no D2915, Sigma) for 2-3 weeks. Cells were then fixed with 10% formalin and stained
450 with 0.5% Oil Red O (Catalog no O1391, Sigma). Chondrogenic differentiation was induced
451 in monolayer culture where cells were cultured with DMEM high glucose containing 10mM
452 HEPES (1M), 100U of penicillin / streptomycin, 10^{-4} M 2-Mercaptoethanol (catalog no.M7522,
453 Sigma), 2mM pyruvate (Catalog no P5280, Sigma), 0.35mM L-proline (Catalog no P5607-
454 25G, Sigma), ITS^{+3} (Catalog no I-3146, Sigma), 5μg/mL L-ascorbic acid 2-phosphate (Catalog
455 no A7506, Sigma), 10^{-7} M dexamethasone (Catalog No D2915, Sigma), and 10ng/mL TGF-β3
456 (Catalog no 100-36E, Peprotech). To assess chondrogenic differentiation, toluidine blue
457 (Catalog no T3260, Sigma) (pH 2.0 to 2.5) was used to stain proteoglycan. Images were then
458 taken under inverted microscope (CKX41, Olympus).

459

460 ***In vitro* chondrogenic induction in micromass pellet**

461 After *in vitro* expansion, $2.5x10^5$ of BM MSCs or skin $Ebf2^+$ or skin $Ebf2^-$PαS MPCs were
462 collected in 15mL tube and spun down at 300g for 7 minutes. After removal of supernatant,
463 500 μM of chondrogenic medium consisting of DMEM high glucose with 10 mM HEPES,
464 100U of penicillin/streptomycin, 10^{-4} M 2-Mercaptoethanol (catalog no.M7522, Sigma), 2 mM
465 pyruvate (Catalog no P5280, Sigma), 0.35 mM L-proline (Catalog no. P5607-25G, Sigma),
466 ITS^{+3} (Catalog no. I-3146, Sigma), 5μg/mL L-ascorbic acid 2-phosphate (Catalog no. A7506,
467 Sigma), 10^{-7}M dexamethasone (Catalog No. D2915, Sigma,), and 10ng/mL TGF-β3 (Catalog
468 no. 100-36E, Peprotech) were added. The chondrogenic induction was performed in 37°C
469 under hypoxic condition (2% O_2). Every 2-3 days, the medium was replaced until day 28. For
470 evaluating the chondrogenic induction, the micromass pellets were washed with PBS prior
471 being fixed in 4% PFA for 2 days. After dehydration with 70% ethanol, the pellets were stained
472 with toluidine blue (Catalog no. T3260, Sigma) at pH 2.0 to 2.5 for 15–30 minutes. Thereafter,
473 the stained pellets were washed with 70% ethanol and embedded in OCT-compound (Catalog
474 no. 4583, Sakura Tissue Tex®,). To visualize the formation of proteoglycan, the embedded
475 pellet was cut to 10μm, mounted and observed by inverted microscope (Axio Observer.Z1,
476 Zeis). Images were processed with Zen software (Carl Zeiss Microscopy, GmbH 2011).

477

478 **Skin MPC expansion and proliferation kinetics *in vitro***

479 For *in vitro* expansion, CFU-Fs from FACS-sorted skin $Ebf2^+$ and $Ebf2^-$PαS cells were
480 trypsinized with 0.05% trypsin-EDTA (GIBCO), collected, and plated to T-25 flasks at 400
481 cells /cm^2. Cells were then expanded in complete Dulbecco modified Eagle Medium (DMEM,
482 catalog no.31966, GIBCO) containing 10% FBS, 10 mM HEPES (1M), 100U of penicillin /
483 streptomycin, and 10^{-4}M 2-Mercaptoethanol (catalog no.M7522, Sigma) under hypoxic
484 condition (1-2% O_2) until 80%-90% confluence was reached. Proliferation rates of skin $Ebf2^+$
485 and $Ebf2^-$PαS cells were evaluated by population doubling time (PDT) assays. PDT was
486 calculated by dividing number of days for culturing the cells with number of population
487 doublings (PDs) using following formula: PDT= Culture time (days)/PD where PD=log
488 (NH/NI)/ log 2, NH is harvested cell number and NI is initial cell number.

489

490 **Dorsal skin wholemount immunofluorescence staining**

491 Dorsal skin specimens were fixed in 4% PFA for 10 minutes followed by washing with PBS
492 prior embedding in OCT-Compound (Sakura Tissue Tex®, Catalog no. 4583). For
493 immunofluorescence staining, 150 μM dorsal skin sections were first blocked with skim milk,
494 fish skin gelatin (Catalog no. G7765, Sigma) and Triton X-100 (Catalog no. T8787, Sigma) for
495 1hour at RT. To visualize Ebf2$^+$ cells in mouse dorsal skin, the sections were incubated with
496 anti-GFP, additionally stained with either anti-mouse MECA32, CD31, NG2, NESTIN, or α-
497 SMA antibodies. All stainings were performed at 2-8°C overnight prior washing with PBS and
498 staining with secondary antibody. Imaging was performed with confocal microscopy at Live
499 Cell Imaging (LCI) facility after the section was mounted in Mountant PermaFlour (Catalog
500 no. TA-030-F19, Thermo). See Table S2 for antibodies used for the confocal imaging.
501 Quantification of the Ebf2$^+$ or Ebf2/GFP$^-$Tomato$^+$ cells expressing NESTIN, NG2 or α-SMA
502 was performed with NIS-element AR-analysis ver 5.20.00 64-bit software (Nikon). From
503 100μM section, 30-40μM thickness was scanned with a confocal microscope to localize Ebf2$^+$
504 and Ebf2$^+$ progenies (Ebf2/GFP$^-$Tomato$^+$ cells). Areas where Ebf2$^+$ and Ebf2/GFP$^-$Tomato$^+$
505 cells were distributed were further imaged every 1-1.1μM depth to obtain Region of interest
506 (ROI). Within ROI, positive expression of NESTIN, NG2 or α-SMA was defined based on
507 control sections stained with secondary antibodies only while GFP$^+$ signal was set based on
508 samples from non-GFP reporter mice. Three to 4 mice were included for the quantification.
509

510 **RNA sequencing**

511 Total RNA from freshly sorted skin Ebf2$^+$ cells, skin Ebf2$^-$ PαS cells and BM MSCs were
512 isolated with RNeasy Micro Kit (Qiagen) according to the manufacturer's protocol. cDNA was
513 prepared using SMART-Seq v4 Ultra Low Input RNA Kit for Sequencing (Cat. No. 634898,
514 Takara Bio.). The cDNA quality was examined on Agilent TapeStation system using a High
515 Sensitivity D5000 ScreenTape (Cat. No. 5067-5592, Agilent). One ng cDNA was used for
516 library preparation using *Nextera XT* DNA Library Preparation Kit (Cat. Nos. FC-131-1024 &
517 FC-131-1096, Illumina). The yield and quality of the amplified libraries were analyzed using
518 Qubit by Thermo Fisher and the Agilent Tapestation System. The indexed cDNA libraries were
519 sequenced on the Illumina 2000 or Nextseq 550 (Illumina, San Diego, CA) for a 75-cycle v2
520 sequencing run generating 75 bp single-end reads. About 7-20 million reads/sample were
521 obtained. Sample quality was assessed using FastQC (v0.11.8) and MultiQC (v1.7). Reads
522 were aligned to a reference built from Ensembl GRCm38 genome sequences using STAR
523 (v2.6.1d). All mapped counts to each gene were further calculated by FeatureCounts function

524 from Subread package [57] installed in R. Genes with Reads Per Kilobase of transcript per Million
525 mapped reads (RPKM) values more than 0.1 were considered as being actively transcribed and
526 proceeded to the analysis of Differential Gene Expression (DGE).[58] The normalized read
527 counts assigned to each sample were generated by Deseq2. The differentially expressed genes
528 between the cell subsets were identified by adjusted *P* value (*p*adj < 0.05) using Benjamini-
529 Hochberg correction for multiple testing, together with thresholds at log_2fold changes >1 (up-
530 regulated) or <-1 (down-regulated). For the Gene Set Enrichment Analysis (GSEA), the
531 normalized read counts were imported into the GSEA (v4.0.3) platform from Broad Institute
532 (http://www.broadinstitute.org/gsea/index.jsp), with three gene sets being tested, including
533 gene ontology (c5.all.v5.symbols.gmt), hallmark (h.all.v5.symbols.gmt) and KEGG
534 (c2.kegg.v5.symbols.gmt). Gene sets tested were considered to be statistically enriched when
535 the nominal P value < .01 and FDR < .25.
536
537 **LIN$^-$SCA1$^+$KIT$^+$ (LSK) CD150$^+$ cell isolation**
538 Mouse femurs, tibia and iliac crest were crushed and washed with PBS/5% FBS to obtain BM
539 mononuclear cells. Hematopoietic lineage (LIN) markers TER119, B220, GR-1, CD3, CD11b
540 were firstly depleted with the use of sheep anti-rat DynaI beads (Invitrogen). LIN-depleted
541 cells were then stained with anti-SCA1, anti-KIT, anti-CD150 and PECY5-conjugated
542 antibodies against the LIN markers mentioned above. After excluding dead cells based on
543 propidium iodiode (PI) staining, the LSKCD150$^+$ HSCs were sorted on BD FACS Aria III (BD
544 Biosciences, San Jose) using DIVA 7.0 software. The gating was defined based on fluorescence
545 minus one (FMO). See table S1 for antibody detail information.
546
547 **Co-culture of skin MPCs with LSKCD150$^+$ cells and colony-forming cell in culture (CFU-**
548 **C) assay**
549 Twenty-five thousand (25,000) expanded Ebf2$^+$ or Ebf2$^-$PαS MPCs from skin and BM at
550 passage 4-13 were plated into each well of 12-well plate and maintained in complete Dulbecco
551 modified Eagle Medium (DMEM, catalog no.31966, GIBCO) containing 10% FBS, 10 mM
552 HEPES (1M), 100U of penicillin/streptomycin and 10^{-4}M 2-Mercaptoethanol (catalog
553 no.M7522, Sigma) under hypoxic condition (2% O_2) for 24h prior co-culture. The co-cultures
554 were started by plating 2000 sorted LSKCD150$^+$ to each well in Myelocult medium (M5300,
555 Stem Cell Technologies) supplemented with 10^{-6} M hydrocortisone (Catalog no 74142, Stem
556 Cell Technologies,) and 1% penicillin streptomycin. After a 3-day co-culture in 5% CO_2 at

557 37°C, the medium containing hematopoietic cells and trypsinized cells were collected for
558 FACS analysis and CFU-C assay in Methylcellulose M3434 (Stem Cell Technologies). After
559 10 days of culture at 37°C in 5% CO_2, CFU-Cs in the methylcellulose were stained with 2,7-
560 diaminofluorene (DAF staining) and scored with an inverted microscope (CKX41, Olympus).
561 A cell cluster with a minimum of 50 cells is defined as one colony. Colonies with positive DAF
562 staining were defined as erythrocytes-containing colonies including CFU-GME and BFU-E),
563 as performed previously.[9 59]
564
565 **Cobblestone area-forming cells (CAFC) assay using primary skin MPCs**
566 This was done as previously described.[60] Briefly, 30.000 skin or BM Ebf2$^+$ or Ebf2$^-$PαS MPCs
567 were first plated into a 24-multiwell plate and maintained in complete Dulbecco modified
568 Eagle Medium (DMEM, catalog no.31966, GIBCO) containing 10% FBS, 10mM HEPES
569 (1M), 100U of penicillin/streptomycin, and 10^{-4}M 2-Mercaptoethanol (catalog
570 no.M7522,Sigma) under hypoxic condition (1% O_2). One day after, 150-300 MLL-AF9 or LSK
571 cells were then added on the MSCs and MPCs in Myelocult (M5300, Stem Cell Technologies)
572 with 10^{-6} M hydrocortisone (Catalog no. 07904, Stem Cell Technologies,), 1% penicillin
573 streptomycin and 1ng/mL IL-3 (R&D). The co-cultures were performed at 32°C in 5% CO_2 for
574 7-14 days. A CAFC was defined as a cluster of more than 3 cells underneath the MSCs/MPCs.
575 The CAFCs were visualized and scored with inverted microscope (CKX41, Olympus) on day
576 7 and 10. At day 10-14, the cells were trypsinized and collected for FACS analysis of the KIT$^+$
577 and CD36$^+$ AML LSCs and their cell cycle status.
578
579 **Detection of reactive oxygen species (ROS) level**
580
581 The MSCs/MPCs or AML cells were harvested and washed with PBS and incubated with 2µM
582 of H_2-DCFDA (C6827, ThermoFisher) in DMEM at 37°C for 40min to detect ROS level. The
583 cells were then rinsed twice with PBS and resuspended with 150µL of Propidium iodide
584 (1:1000) in 5%FBS/PBS. ROS levels were measured by FACS.
585
586 **Mitochondrial transfer**
587 MSCs or MPCs were stained with 100nM MitoTracker™ red FM (M22426, ThermoFisher) at
588 37°C for 60 min, according to the manufacturer's instructions. The cells were washed twice
589 with PBS, then incubated for 3-4 hours to remove unbound probe before a final wash.
590 Subsequently, 15,000-25,000 MLL-AF9 AML cells in Myelocult (M5300, StemCell

591 Technologies) were plated and cocultured with prelabelled MSCs for 24 hours. Mitochondrial
592 transfer was quantified in AML cells (CD45.1^{+}) by FACS and analyzed for MFI of the
593 mitoTracker red.
594
595
596 **Colony-forming unit-fibroblast (CFU-F), RNA sequencing** and **quantitative RT-PCR (Q-**
597 **PCR)** were done as described.[6,35] See Table S3 for information of Assays-on-Demand probes.
598

599 **Statistical analysis**

600 Unless mentioned, either unpaired t-test or Mann-Whitney test was used to determine the
601 difference between the groups or cell subsets. All statistical tests were performed with
602 GraphPad Prism 8 software with $P < 0.05$ considered statistically significant.
603

604 **Data availability**

605 The RNA sequencing data are available at GEO under accession number GSE167562.
606

607 **Acknowledgements**

608 We thank Tina Jacob, Karl Annusver and Alexandra Are at Department of Cell and Molecular
609 Biology, Karolinska Institute, Sweden for valuable advice and technical discussion. We thank
610 Alexandre Piccini, Yuanyuan Zhang and Andranik Durguryan in our group for technical help
611 for the cell culture. We also thank Prof. Marja Ekblom, Lund University for her scientific input.
612 This study was supported by the Swedish Research Council (2019-01361), Swedish Childhood
613 Cancer Society (PR2015-0142, FoAss13/015, PR2017/0154, PR2020-0166), Swedish Cancer
614 Society (CAN2017/774, 19 0092 SIA and 20 1222PjF), Åke Olsson foundation,
615 Radiumhemmets Forskningsfonder (151241, 171162, 191253) and Karolinska Institute
616 Wallenberg Institute for Regenerative Medicine, Karolinska Institute doctoral education (KID)
617 funding (2-1293/2014) to support LS, Stiftelsen Clas Groschinskys Minnesfond (ref:M16 50)
618 to H.Q., and the Swedish Research Council (2018-02963) and Swedish Cancer Society (CAN
619 2018/793) to MK. FACS analysis and cell sorting were performed at MedH Flow Cytometry
620 core facility (Karolinska Institute), supported by KI/SLL. The confocal images were obtained
621 at the LCI facility/Nikon Center of Excellence, Karolinska Institute, supported by grants from
622 the Knut and Alice Wallenberg Foundation, the Swedish Research Council, KI infrastructure,

Centre for Innovative Medicine and Jonasson center at the Royal Institute of Technology. All major computations were performed on resources provided by the Swedish National Infrastructure for Computing (SNIC) through Uppsala Multidisciplinary Center for Advanced Computational Science (UPPMAX) under Project sens2018540. We also would like to thank the core facility at NEO, BEA, Bioinformatics and Expression Analysis, which is supported by the board of research at the Karolinska Institute and the research committee at the Karolinska Hospital.

Author contributions

LS has substantially participated in designing, performing experiments, collecting and analyzing data and manuscript writing. HC, PX, MK(Kondo), XS, EL and ASJ performed experiments, collected data and assisted with data analysis and manuscript-editing. MK (Kasper) provided scientific input and assistance with confocal imaging of skin tissues. MJ provided the DsRed-expressing MLL-AF9 AML cells and scientific input on the manuscript. KT provided Lama4$^{-/-}$ mouse models and scientific input. HQ designed, performed experiments, collected and analyzed data, wrote the manuscript. All authors have proved the final version of the manuscript.

Conflict of interest: All authors declare no competing financial interest regarding this study.

References

1 Bakst, R. L., Tallman, M. S., Douer, D. & Yahalom, J. How I treat extramedullary acute myeloid leukemia. *Blood* **118**, 3785-3793, doi:10.1182/blood-2011-04-347229 (2011).

2 Gouache, E. *et al.* Leukemia Cutis in Childhood Acute Myeloid Leukemia: Epidemiological, Clinical, Biological, and Prognostic Characteristics of Patients Included in the ELAM02 Study. *Hemasphere* **2**, e141, doi:10.1097/HS9.0000000000000141 (2018).

3 Wang, C. X., Pusic, I. & Anadkat, M. J. Association of Leukemia Cutis With Survival in Acute Myeloid Leukemia. *JAMA Dermatol* **155**, 826-832, doi:10.1001/jamadermatol.2019.0052 (2019).

4 Krooks, J. A. & Weatherall, A. G. Leukemia cutis in acute myeloid leukemia signifies a poor prognosis. *Cutis* **102**, 266;271;272 (2018).

656 5 Hoggatt, J., Kfoury, Y. & Scadden, D. T. Hematopoietic Stem Cell Niche in Health and
657 Disease. *Annual review of pathology* **11**, 555-581, doi:10.1146/annurev-pathol-
658 012615-044414 (2016).
659 6 Xiao, P. *et al.* Distinct roles of mesenchymal stem and progenitor cells during the
660 development of acute myeloid leukemia in mice. *Blood advances* **2**, 1480-1494,
661 doi:10.1182/bloodadvances.2017013870 (2018).
662 7 Raaijmakers, M. H. *et al.* Bone progenitor dysfunction induces myelodysplasia and
663 secondary leukaemia. *Nature* **464**, 852-857, doi:nature08851 [pii]
664 10.1038/nature08851 (2010).
665 8 Dong, L. *et al.* Leukaemogenic effects of Ptpn11 activating mutations in the stem
666 cell microenvironment. *Nature* **539**, 304-308, doi:10.1038/nature20131 (2016).
667 9 Xiao, P. *et al.* Sipa1 deficiency-induced bone marrow niche alterations lead to the
668 initiation of myeloproliferative neoplasm. *Blood advances* **2**, 534-548,
669 doi:10.1182/bloodadvances.2017013599 (2018).
670 10 Hanoun, M. *et al.* Acute myelogenous leukemia-induced sympathetic neuropathy
671 promotes malignancy in an altered hematopoietic stem cell niche. *Cell stem cell* **15**,
672 365-375, doi:10.1016/j.stem.2014.06.020 (2014).
673 11 Schepers, K. *et al.* Myeloproliferative neoplasia remodels the endosteal bone
674 marrow niche into a self-reinforcing leukemic niche. *Cell Stem Cell* **13**, 285-299,
675 doi:10.1016/j.stem.2013.06.009 (2013).
676 12 Kim, J. A. *et al.* Microenvironmental remodeling as a parameter and prognostic
677 factor of heterogeneous leukemogenesis in acute myeloid leukemia. *Cancer Res*,
678 doi:10.1158/0008-5472.CAN-14-3379 (2015).
679 13 Jeong, S. Y., Kim, J. A. & Oh, I. H. The Adaptive Remodeling of Stem Cell Niche in
680 Stimulated Bone Marrow Counteracts the Leukemic Niche. *Stem Cells*,
681 doi:10.1002/stem.2870 (2018).
682 14 Han, J. *et al.* Adipose tissue is an extramedullary reservoir for functional
683 hematopoietic stem and progenitor cells. *Blood* **115**, 957-964, doi:10.1182/blood-
684 2009-05-219923 (2010).
685 15 Ye, H. *et al.* Leukemic Stem Cells Evade Chemotherapy by Metabolic Adaptation to
686 an Adipose Tissue Niche. *Cell Stem Cell* **19**, 23-37, doi:10.1016/j.stem.2016.06.001
687 (2016).
688 16 Toma, J. G. *et al.* Isolation of multipotent adult stem cells from the dermis of
689 mammalian skin. *Nat Cell Biol* **3**, 778-784, doi:Doi 10.1038/Ncb0901-778 (2001).
690 17 Kimlin, L. & Virador, V. Cellular populations isolated from newborn mouse skin
691 including mesenchymal stem cells. *Methods in molecular biology* **989**, 217-233,
692 doi:10.1007/978-1-62703-330-5_17 (2013).
693 18 Viswanathan, S. *et al.* Mesenchymal stem versus stromal cells: International
694 Society for Cell & Gene Therapy (ISCT(R)) Mesenchymal Stromal Cell committee
695 position statement on nomenclature. *Cytotherapy* **21**, 1019-1024,
696 doi:10.1016/j.jcyt.2019.08.002 (2019).
697 19 Vaculik, C. *et al.* Human dermis harbors distinct mesenchymal stromal cell subsets.
698 *J Invest Dermatol* **132**, 563-574, doi:10.1038/jid.2011.355 (2012).
699 20 Morikawa, S. *et al.* Prospective identification, isolation, and systemic
700 transplantation of multipotent mesenchymal stem cells in murine bone marrow. *J*
701 *Exp Med* **206**, 2483-2496, doi:jem.20091046 [pii]
702 10.1084/jem.20091046 (2009).

703 21 Pinho, S. *et al.* PDGFRalpha and CD51 mark human Nestin+ sphere-forming
704 mesenchymal stem cells capable of hematopoietic progenitor cell expansion. *J Exp*
705 *Med* **210**, 1351-1367, doi:10.1084/jem.20122252 (2013).
706 22 Qian, H. *et al.* Molecular characterization of prospectively isolated multipotent
707 mesenchymal progenitors provides new insight into the cellular identity of
708 mesenchymal stem cells in mouse bone marrow. *Molecular and cellular biology* **33**,
709 661-677, doi:10.1128/MCB.01287-12 (2013).
710 23 Armulik, A., Genove, G. & Betsholtz, C. Pericytes: developmental, physiological, and
711 pathological perspectives, problems, and promises. *Developmental cell* **21**, 193-
712 215, doi:10.1016/j.devcel.2011.07.001 (2011).
713 24 Kusumbe, A. P. *et al.* Age-dependent modulation of vascular niches for
714 haematopoietic stem cells. *Nature* **532**, 380-384, doi:10.1038/nature17638
715 (2016).
716 25 Baryawno, N. *et al.* A Cellular Taxonomy of the Bone Marrow Stroma in
717 Homeostasis and Leukemia. *Cell* **177**, 1915-1932 e1916,
718 doi:10.1016/j.cell.2019.04.040 (2019).
719 26 Alonso, S. *et al.* Human bone marrow niche chemoprotection mediated by
720 cytochrome P450 enzymes. *Oncotarget* **6**, 14905-14912 (2015).
721 27 Jin, L. *et al.* CXCR4 up-regulation by imatinib induces chronic myelogenous
722 leukemia (CML) cell migration to bone marrow stroma and promotes survival of
723 quiescent CML cells. *Mol Cancer Ther* **7**, 48-58, doi:10.1158/1535-7163.MCT-07-
724 0042 (2008).
725 28 Iwamoto, S., Mihara, K., Downing, J. R., Pui, C. H. & Campana, D. Mesenchymal cells
726 regulate the response of acute lymphoblastic leukemia cells to asparaginase. *J Clin*
727 *Invest* **117**, 1049-1057, doi:10.1172/JCI30235 (2007).
728 29 Zhang, B. *et al.* Microenvironmental protection of CML stem and progenitor cells
729 from tyrosine kinase inhibitors through N-cadherin and Wnt-beta-catenin
730 signaling. *Blood* **121**, 1824-1838, doi:10.1182/blood-2012-02-412890 (2013).
731 30 Xu, X. *et al.* BM microenvironmental protection of CML cells from imatinib through
732 Stat5/NF-kappaB signaling and reversal by Wogonin. *Oncotarget* **7**, 24436-24454,
733 doi:10.18632/oncotarget.8332 (2016).
734 31 Somervaille, T. C. & Cleary, M. L. Identification and characterization of leukemia
735 stem cells in murine MLL-AF9 acute myeloid leukemia. *Cancer Cell* **10**, 257-268,
736 doi:10.1016/j.ccr.2006.08.020 (2006).
737 32 Landberg, N. *et al.* CD36 defines primitive chronic myeloid leukemia cells less
738 responsive to imatinib but vulnerable to antibody-based therapeutic targeting.
739 *Haematologica* **103**, 447-455, doi:10.3324/haematol.2017.169946 (2018).
740 33 Farge, T. *et al.* Chemotherapy-Resistant Human Acute Myeloid Leukemia Cells Are
741 Not Enriched for Leukemic Stem Cells but Require Oxidative Metabolism. *Cancer*
742 *discovery* **7**, 716-735, doi:10.1158/2159-8290.CD-16-0441 (2017).
743 34 Duarte, D. *et al.* Inhibition of Endosteal Vascular Niche Remodeling Rescues
744 Hematopoietic Stem Cell Loss in AML. *Cell Stem Cell* **22**, 64-77 e66,
745 doi:10.1016/j.stem.2017.11.006 (2018).
746 35 Cai, H. *et al.* Critical Role of Lama4 for Hematopoiesis Regeneration and Acute
747 Myeloid Leukemia Progression. *Blood*, doi:10.1182/blood.2021011510 (2021).
748 36 Ahsberg, J. *et al.* Progression of progenitor B-cell leukemia is associated with
749 alterations of the bone marrow micro-environment. *Haematologica* **105**, e102-
750 e106, doi:10.3324/haematol.2018.214031 (2020).

751 37 Poulos, M. G. *et al.* Endothelial Jagged-1 is necessary for homeostatic and
752 regenerative hematopoiesis. *Cell reports* **4**, 1022-1034,
753 doi:10.1016/j.celrep.2013.07.048 (2013).
754 38 Calvi, L. M. *et al.* Osteoblastic cells regulate the haematopoietic stem cell niche.
755 *Nature* **425**, 841-846 (2003).
756 39 Greenbaum, A. *et al.* CXCL12 in early mesenchymal progenitors is required for
757 haematopoietic stem-cell maintenance. *Nature* **495**, 227-230,
758 doi:10.1038/nature11926 (2013).
759 40 Omatsu, Y. *et al.* The essential functions of adipo-osteogenic progenitors as the
760 hematopoietic stem and progenitor cell niche. *Immunity* **33**, 387-399,
761 doi:10.1016/j.immuni.2010.08.017 (2010).
762 41 Arai, F. *et al.* Tie2/angiopoietin-1 signaling regulates hematopoietic stem cell
763 quiescence in the bone marrow niche. *Cell* **118**, 149-161 (2004).
764 42 Thoren, L. A. *et al.* Kit regulates maintenance of quiescent hematopoietic stem
765 cells. *J Immunol* **180**, 2045-2053 (2008).
766 43 Gu, Y. C. *et al.* Laminin isoform-specific promotion of adhesion and migration of
767 human bone marrow progenitor cells. *Blood* **101**, 877-885 (2003).
768 44 Susek, K. H. *et al.* Bone marrow laminins influence hematopoietic stem and
769 progenitor cell cycling and homing to the bone marrow. *Matrix Biol* **67**, 47-62,
770 doi:10.1016/j.matbio.2018.01.007 (2018).
771 45 Stier, S. *et al.* Osteopontin is a hematopoietic stem cell niche component that
772 negatively regulates stem cell pool size. *J Exp Med* **201**, 1781-1791 (2005).
773 46 Batsivari, A. *et al.* Dynamic responses of the haematopoietic stem cell niche to
774 diverse stresses. *Nat Cell Biol* **22**, 7-17, doi:10.1038/s41556-019-0444-9 (2020).
775 47 Moschoi, R. *et al.* Protective mitochondrial transfer from bone marrow stromal
776 cells to acute myeloid leukemic cells during chemotherapy. *Blood* **128**, 253-264,
777 doi:10.1182/blood-2015-07-655860 (2016).
778 48 Marlein, C. R. *et al.* NADPH oxidase-2 derived superoxide drives mitochondrial
779 transfer from bone marrow stromal cells to leukemic blasts. *Blood* **130**, 1649-
780 1660, doi:10.1182/blood-2017-03-772939 (2017).
781 49 Qian, H., Le Blanc, K. & Sigvardsson, M. Primary mesenchymal stem and progenitor
782 cells from bone marrow lack expression of CD44 protein. *The Journal of biological*
783 *chemistry* **287**, 25795-25807, doi:10.1074/jbc.M112.339622 (2012).
784 50 Qian, H. *et al.* Molecular characterization of prospectively isolated multipotent
785 mesenchymal progenitors provides new insight into the cellular identity of
786 mesenchymal stem cells in mouse bone marrow. *Mol Cell Biol* **33**, 661-677,
787 doi:10.1128/MCB.01287-12 (2013).
788 51 Wang, W. *et al.* Aberrant Notch Signaling in the Bone Marrow Microenvironment
789 of Acute Lymphoid Leukemia Suppresses Osteoblast-Mediated Support of
790 Hematopoietic Niche Function. *Cancer Res* **76**, 1641-1652, doi:10.1158/0008-
791 5472.CAN-15-2092 (2016).
792 52 Parsi, M., Go, M. S. & Ahmed, A. in *StatPearls* (2020).
793 53 Forte, D. *et al.* Bone Marrow Mesenchymal Stem Cells Support Acute Myeloid
794 Leukemia Bioenergetics and Enhance Antioxidant Defense and Escape from
795 Chemotherapy. *Cell Metab*, doi:10.1016/j.cmet.2020.09.001 (2020).
796 54 Kode, A. *et al.* FoxO1-dependent induction of acute myeloid leukemia by
797 osteoblasts in mice. *Leukemia* **30**, 1-13, doi:10.1038/leu.2015.161 (2016).
798 55 Thyboll, J. *et al.* Deletion of the laminin alpha4 chain leads to impaired microvessel
799 maturation. *Mol Cell Biol* **22**, 1194-1202 (2002).

56 Hartwell, K. A. *et al.* Niche-based screening identifies small-molecule inhibitors of leukemia stem cells. *Nat Chem Biol* **9**, 840-848, doi:10.1038/nchembio.1367 (2013).

57 Liao, Y., Smyth, G. K. & Shi, W. The Subread aligner: fast, accurate and scalable read mapping by seed-and-vote. *Nucleic acids research* **41**, e108, doi:10.1093/nar/gkt214 (2013).

58 Mortazavi, A., Williams, B. A., McCue, K., Schaeffer, L. & Wold, B. Mapping and quantifying mammalian transcriptomes by RNA-Seq. *Nat Methods* **5**, 621-628, doi:10.1038/nmeth.1226 (2008).

59 McGuckin, C. P., Forraz, N. & Liu, W. M. Diaminofluorene stain detects erythroid differentiation in immature haemopoietic cells treated with EPO, IL-3, SCF, TGFbeta1, MIP-1alpha and IFNgamma. *European journal of haematology* **70**, 106-114 (2003).

60 van Os, R. P., Dethmers-Ausema, B. & de Haan, G. In vitro assays for cobblestone area-forming cells, LTC-IC, and CFU-C. *Methods Mol Biol* **430**, 143-157, doi:10.1007/978-1-59745-182-6_10 (2008).

Figure Legends

Figure 1 AML cells infiltrated in skin are capable to regenerate AML post-transplantation

(**A**) Strategy to generate MLL-AF9 AML mouse model. MLL-AF9 transduced AML cells expressing CD45.1 were transplanted into non-irradiated CD45.2 C57BL/6 mice.

(**B**) FACS profile showing AML engraftment analysis in BM, peripheral blood (PB) and dorsal skin at the end stage of AML. The numbers in the panel are the mean frequencies.

(**C**) Proportion of the AML cells within total hematopoietic ($CD45^+$) cell in dorsal skin and PB. Data were from 6 independent experiments and each dot represents data from a mouse. The horizontal bars represent mean values. Paired t-test was used for statistical analysis.

(**D**) Distribution of MLL-$AF9^+$ AML cells expressing DsRed at perivascular sites in dorsal skin. The endothelial cells were marked by CD31 expression (white).

(**E**) Experimental strategy to test AML-initiating capacity of the AML cells infiltrated in mouse skin by serial transplantation. The primary recipient mice (CD45.2) that developed AML post-AML cell (CD45.1) transplantation were treated with Ara-C or saline (NS, untreated). The residual $CD45.1^+$ AML cells from skin were sorted at 2-3days after the last injection of Ara-C and transplanted into secondary non-irradiated CD45.2 C57BL/6 mice at doses of 1000 (1K)-5000 (5K) cells/mouse, respectively. The AML development was monitored by FACS and hematology analyzer Sysmex. The mice were sacrificed when found dead or moribund.

838 (**F**) The Kaplan-Meier survival curve of the secondary recipient mice which received skin-
839 derived AML cells sorted from primary recipients after treatment with Ara-C or normal saline.
840 The date was the time when the mice were found dead or moribund. The survival curve was
841 generated by Log-rank (Mantel-Cox test).
842 (**G**) Platelet counts in PB of the secondary recipient mice at the endpoint.
843 (**H**) FACS profile showing the engraftment of skin-derived AML CD45.1$^+$ cells in BM of the
844 secondary recipient mice.
845 (**I**) The engraftment levels of the skin-derived AML CD45.1$^+$ cells in BM of the secondary
846 recipient mice.
847 (**J**) Spleen size of the recipient mice at the endpoint.
848 (**K**) The frequencies of the secondary mice that developed AML after injection of skin-derived
849 AML cells.
850
851 **Figure 2 Identification of skin MPC subsets by Ebf2 expression.**
852 (**A**) A representative FACS profile showing FACS sorting/analysis of the Ebf2$^+$ and Ebf2$^-$ cells
853 in dorsal skin. The cells were first gated within non-hematopoietic (CD45$^-$TER119$^-$) and non-
854 endothelial (CD31$^-$) live (PI$^-$) stromal cells. Then, these cells lacking expression of CD44 were
855 further analyzed for their expression of SCA1, PDGFRa/CD140a (PαS) and CD51. The
856 numbers in the panel are the mean frequencies.
857 (**B-C**) The Ebf2$^+$ cell frequency within total PI$^-$ (**B**) or PI$^-$CD45$^-$TER119$^-$CD31$^-$ stromal cells
858 (**C**) in dorsal skin.
859 (**D**) The fractions of PαS cells within the Ebf2$^+$ and Ebf2$^-$ stromal cells. Each dot in **B-D**
860 represents data from a single mouse in 3-6 experiments with the horizontal line as a mean value.
861 (**E**) CFU-Fs in the Ebf2$^+$ and Ebf2$^-$ stromal cells.
862 (**F**) CFU-Fs were exclusively found in the Ebf2$^+$SCA1$^+$ cell fraction. Data in **E-F** are from 3
863 independent experiments and each dot represents replicate assays from 2-3 mice in each
864 experiment. The horizontal line represents mean value. Wilcoxon matched-signed pair rank
865 test was used for statistical analysis.
866 **(G-J)** Single-cell analysis of CFU-Fs and lineage differentiation from the FACS-sorted Ebf2$^+$
867 (**G-H**) and Ebf2$^-$PαS (**I-J**) stromal cells. The CFU-F frequencies (**G**, **I**) were determined by
868 limiting dilution at a density of 1, 2, 5, 10 cells per well in a 96-well plate and the frequency
869 of the single cells with bi-lineage plasticity (**H, J**) were assessed by multilineage differentiation
870 potential of single CFU-Fs derived from the cells.

871 (**K**) Representative images of the osteogenic and adipogenic differentiation from single CFU-
872 F clones derived from Ebf2$^+$ and Ebf2$^-$PαS cells.
873 (**L**) Population-doubling time (PDT) of randomly selected CFU-Fs derived from single Ebf2$^+$
874 and Ebf2$^-$PαS cells. Each line represents the growth kinetics of a single clone.
875 See also in Figure S1.
876
877 **Figure 3 Distribution and hierarchical relationship of skin MPCs.**
878 (**A**) Localization of Ebf2$^+$ cells in skin perivascular area (Box 1) and in dermal panniculus
879 carnosus (DPC). The endothelial cells in the vessels were identified by MECA32 staining.
880 (**B**) Representative image showing the perivascular localization of Ebf2$^+$ cells adjacent to
881 CD31$^+$ endothelial cells in dorsal skin.
882 (**C**) A scheme showing strategy for lineage-tracing of the Ebf2$^+$ cells in skin. The
883 Ebf2/GFP$^+$Tomato$^+$ cells and their progenies (Ebf2/GFP$^-$Tomato$^+$) were traced by FACS at 3,
884 6, 12 months after tamoxifen injection.
885 (**D**) A representative FACS profile showing analysis of activated Ebf2$^+$ cells (GFP$^+$Tomato$^+$)
886 and their progeny (GFP$^-$Tomato$^+$). The gates for different cell subsets were defined with FMO
887 from bi-transgenic or single transgenic mice. Each stromal cell subset (PI$^-$CD45$^-$TER119$^-$
888 CD31$^-$) was gated within the CD44$^-$ fractions and subsequently gated for PαS cells based on
889 CD140a and SCA1 expression.
890 (**E**) The frequencies of Ebf2/GFP$^+$Tomato$^+$ cells and its progenies (Ebf2/GFP$^-$Tomato$^+$) within
891 stromal cells.
892 (**F**) The fractions of PαS and Ebf2$^-$CD140a$^+$SCA1$^-$ cells within total GFP$^-$Tomato$^+$ cells
893 generated by Ebf2$^+$ cells. Each dot represents data from each mouse from 2-3 independent
894 experiments. Horizontal bars represent the mean., and unpaired *t*-test were used for statistical
895 analysis.
896 (**G**) Distribution of the single Ebf2/GFP$^+$Tomato$^-$ cells (green), activated Ebf2/GFP$^+$Tomato$^+$
897 cells (orange) and Ebf2/GFP$^-$Tomato$^+$ (red) cells at 3 months after tamoxifen injection.
898 See also in Figure S2-S3.
899
900 **Figure 4 Skin MPCs support AML LSC growth and protect them from chemotherapy.**
901 (**A**) Experimental strategy for assessing the role of the skin MPC and BM MSC subsets for
902 AML growth by cobblestone area-forming cell (CAFC) assay.
903 (**B**) Representative images of CAFCs derived from the AML cells.

904 (**C**) Total numbers of CAFCs generated from 150 MLL-AF9$^+$ AML cells.
905 (**D**) A proportion of residual CAFCs from AML cells after Ara-C treatment relative to the
906 normal saline (NS)-treated controls.
907 (**E**) The total number of the AML cells at 10 days after Ara-C treatment.
908 (**F-G**) The frequency (F) and the numbers (G) of the KIT$^+$ AML LSCs.
909 (**H-I**) The frequency (H) and the numbers (I) of the CD36$^+$ chemoresistant AML cells.
910 Data in C-I were from 3-4 independent experiments and each dot represents the mean of
911 replicate assays. The horizontal bars represent mean values. Unpaired (C-E, G, I) or paired
912 (F,H) *t*-test was used for statistical analysis.
913 (**J**) Co-localization of AML cells (red) with the Ebf2$^+$ cells. Ebf2 was determined by GFP
914 (green) and the endothelial cells were marked by CD31 (white).
915 (**K**) Representative FACS plot showing analysis of Ebf2$^+$ MPCs in AML mouse dorsal skin.
916 (**L**) The frequency of the Ebf2$^+$ MPCs within stromal cells in dorsal skin tissue at endstage of
917 AML. Data were from 6 independent experiments and each dot represents a mouse. The
918 horizontal bars represent mean values. Unpaired t-test was used for statistical analysis.
919 (**M**) Representative FACS plot showing analysis of the skin Ebf2$^-$PαS MPCs in healthy
920 controls and AML mice.
921 (**N**) The frequency of the Ebf2$^-$PαS cells within stromal cells in dorsal skin at the end stage of
922 AML. Data were from 6 independent experiments and each dot represents a mouse. The
923 horizontal bars represent mean values. Unpaired t-test or Mann-Whitney was used for
924 statistical analysis.
925 (**O**) FACS profile showing analysis of CD31$^+$ cells in the dorsal skin of healthy and AML mice.
926 (**P**) The frequency of total endothelial cells (CD31$^+$) and arteriolar endothelial cells
927 (CD31$^+$SCA1$^+$).
928
929 **Figure 5 RNA sequencing revealed the molecular profile of skin Ebf2$^+$ and Ebf2$^-$PαS**
930 **MPCs.**
931 (**A**) Venn diagram showing differentially expressed genes (DEG) among the skin Ebf2$^+$ MPCs,
932 skin Ebf2$^-$PαS MPCs and BM MSCs.
933 (**B**) Gene set enrichment analysis (GSEA) revealed the enrichment of genes associated with
934 different biological processes and cellular responses in the skin Ebf2$^+$ and Ebf2$^-$PαS MPC
935 subsets.

936 (**C**) A volcano plot showing differentially expressed genes between skin MPCs (Ebf2$^+$ and
937 Ebf2$^-$PαS) and BM MSCs.
938 (**D**) GSEA revealed the enrichment of gene sets associated with various biological processes
939 and cellular responses in the skin MPCs (Ebf2$^+$ and Ebf2$^-$PαS) and BM MSCs.
940 (**E**) GSEA plots showing the enrichment of genes related to oxidative phosphorylation,
941 inflammatory and interferon alpha response in the skin MPCs compared to that in BM MSCs.
942 FDR (false discovery rate) and *P* values are indicated in the panels.
943 (**F**) Heatmap showing the expressions of selected inflammatory cytokines in skin Ebf2$^+$ cells,
944 Ebf2$^-$PαS cells and BM MSCs. The heatmap was created in Excel using conditional formatting.
945 The color scale was set based on the minimum, midpoint and maximum values of each gene in
946 each row. Red correlates with high expression and green correlates with low expression.
947 (**G**) Gene sets enrichment plot showing hematopoiesis supportive niche genes in skin MPC
948 subsets and BM MSCs, and the heatmap showing the gene expression levels.
949 (**H**) Q-PCR of HSC niche genes in BM MSCs, skin Ebf2$^+$ and Ebf2$^-$PαS MPCs. Each dot
950 represents mean of triplicate measurement of the gene expression relative to *Hprt*. Horizontal
951 bars represent the mean values. Data were from 3 independent sorting experiments. Unpaired
952 *t*-tests were used as statistical analysis.
953 See also in Figure S4.
954
955 **Figure 6 Mitochondrial transfer and Lama4 deficiency in skin MPCs contributed to the**
956 **chemoprotection of AML cells from Ara-C.**
957 (**A**) Experimental strategy for determining mitochondrial transfer from stromal cells to AML
958 cells *in vitro*. Skin MPCs and BM MSCs that were prelabelled with MitoTracker red were co-
959 cultured with MLL-AF9$^+$ AML cells for 24 hours. Ara-C was added 4-6 hours after seeding
960 the AML cells.
961 (**B**) Mean fluorescence intensity (MFI) of MitoTracker showing mitochondrial transfer from
962 the stromal cells to AML cells in the cocultures. The AML cells were co-cultured with BM
963 MSCs and skin PαS MPCs pre-labeled with MitoTracker red. The stromal cell-derived
964 mitochondria were detected by MFI of MitoTracker in the AML cells at 24h post-coculture by
965 FACS. Data shown are normalized MitoTracker MFI in the AML cells based on the values of
966 that in the AML co-cultured with BM MSCs without Ara-C treatment. Each dot represents
967 mean values of 3-4 replicated measurements in each experiment of 4. Horizontal bars are
968 median values.

969 (**C**) Representative FACS histograms showing MitoTracker MFI in the AML cells 24h post
970 coculture with the stromal cells. The MFI from AML cells in the monoculture without the
971 prelabeled MPCs was used as a negative control.
972 (**D**) ROS levels in the AML cells cocultured with BM MSCs or skin PαS MPCs 24h post-Ara-
973 C treatment. Each dot represents the average value of triplicate assays from each experiment
974 of 3. Horizontal bars are mean values.
975 (**E**) The % of PI^- live AML cells in the cocultures 24h after Ara-C treatment. Each dot
976 represents mean values of 3-4 replicated measurements in each experiment of 4. Horizontal
977 bars are median values.
978 The statistical differences in (B-E) among different types of cultures were determined by
979 unpaired *t* test, and between NS and Ara-C treated groups within the same type of co-cultures
980 were analyzed by paired t test.
981 (**F**) Experimental layout for assessing the impact of *Lama4* loss in skin MPCs for AML growth
982 *in vitro* using a co-culture system. The *Lama4*$^{+/+}$ and *Lama4*$^{-/-}$ skin MPCs were co-cultured
983 with MLL-AF9 AML cells in a 96-well plate. For CAFC assay, Ara-C was added 2 days post-
984 seeding of AML cells. The numbers of total AML cells and CAFCs were counted at 24-28h
985 and day 7 post-seeding AML cells, respectively.
986 (**G**) Fold changes in the number of the AML cells in the co-cultures with *Lama4*$^{-/-}$ skin MPCs
987 in relation to that with *Lama4*$^{+/+}$ MPCs 24hours after Ara-C or saline treatment. Data were
988 from 4 independent experiments and each dot represents the mean of triplicate assays. The
989 horizontal bars represent mean values. Paired *t*-test was used for statistical analysis.
990 (**H**) The number of CAFCs derived from AML cells in the co-cultures with *Lama4*$^{+/+}$ and
991 *Lama4*$^{-/-}$ skin MPCs treated with NS or Ara-C. Data shown are triplicate values from 2-3
992 independent experiments. The horizontal bars represent mean values. Unpaired *t*-test was used
993 for statistical analysis.
994
995 **Figure 7 A high level of residual AML cell infiltration in skin tissue of AML-promoting**
996 ***Lama4*$^{-/-}$ mouse model post Ara-C treatment**.
997 (**A**) Experimental setup. *Lam4*$^{+/+}$ and *Lama4*$^{-/-}$ mice were treated with normal saline (NS) or
998 Ara-C at day 15 after injection of DsRed-expressing MLL-AF9$^+$ AML cells. Peripheral blood
999 (PB) and BM were collected for FACS and confocal microscopy at 1-day after NS or Ara-C
1000 treatment.
1001 (**B**) Representative confocal images showing residual AML cells in dorsal skin at 1-day post-
1002 Ara-C treatment.

1003 (**C**) Frequency of AML cells in PB and skin at 1-day post-Ara-C treatment.
1004 (**D**) Proportion of $CD36^+$ and KIT^+ AML LSCs in skin at 1-day post-Ara-C treatment.
1005 Data were from 2-5 experiments and each dot in C-D represents data from a single mouse. The
1006 horizontal bars represent the mean values. Unpaired *t*-test was used for statistical analysis.
1007 See also in Figure S6.
1008

Figure 1

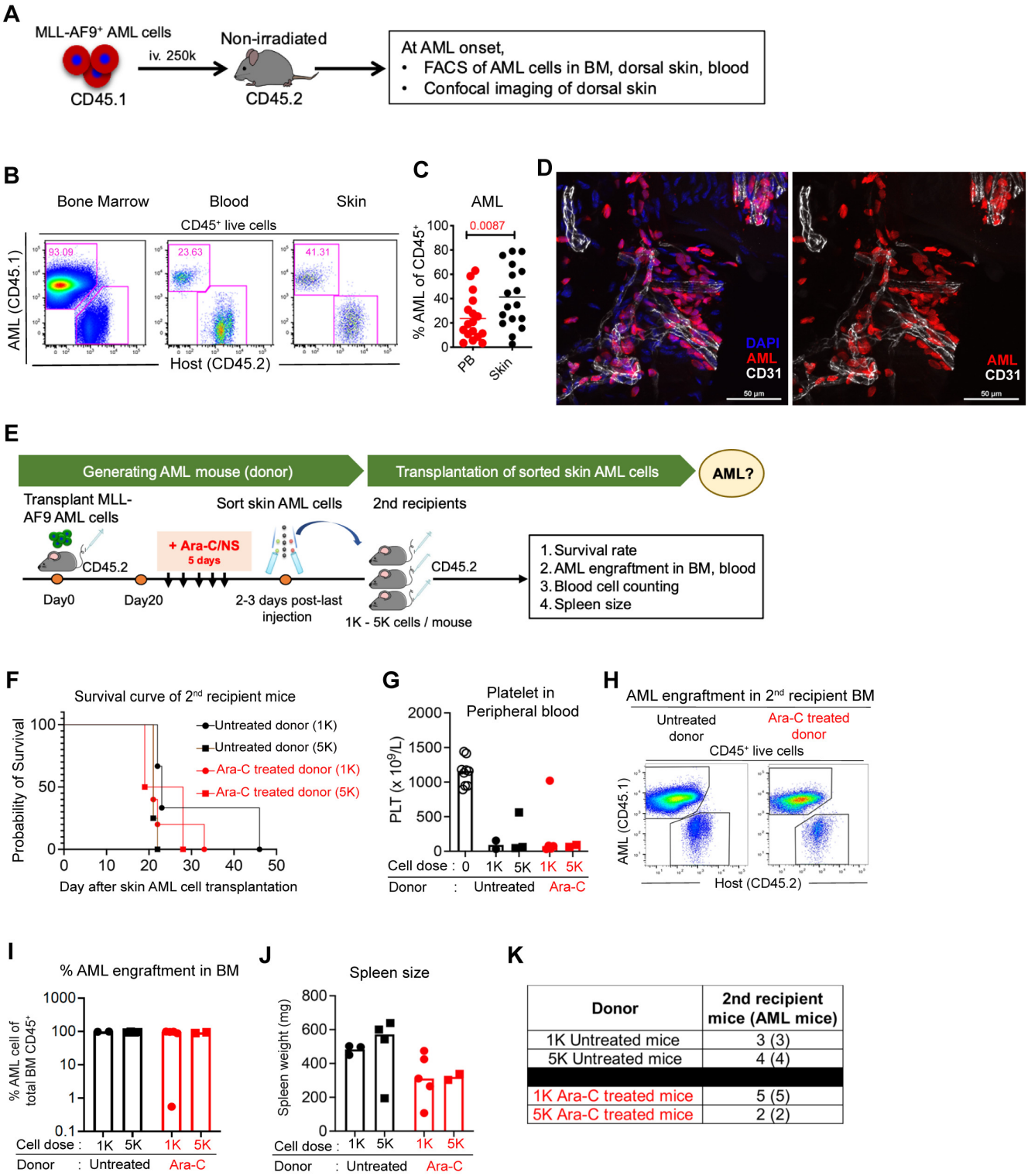

Donor	2nd recipient mice (AML mice)
1K Untreated mice	3 (3)
5K Untreated mice	4 (4)
1K Ara-C treated mice	5 (5)
5K Ara-C treated mice	2 (2)

Figure 2

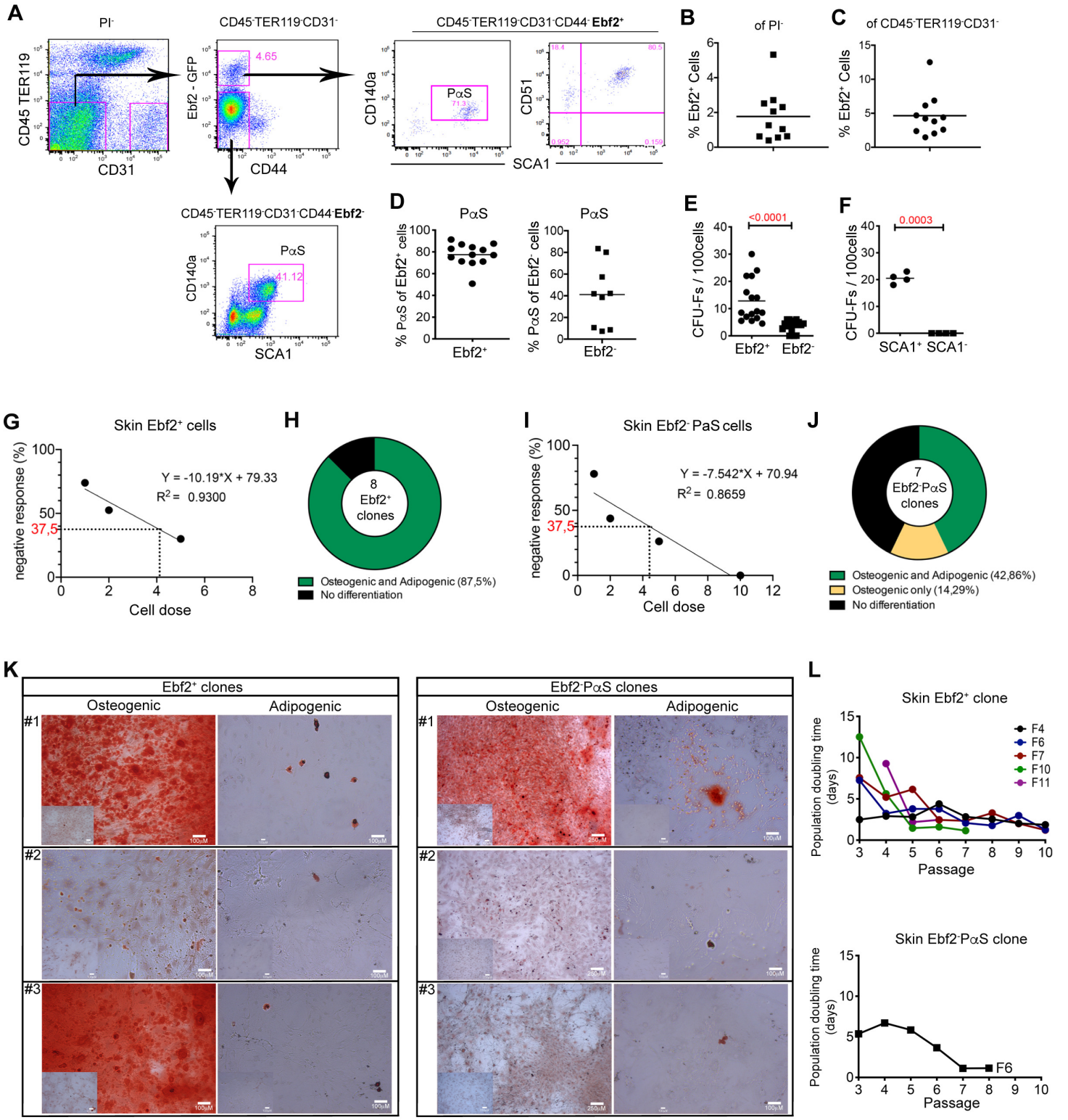
A
PI-
CD45 TER119
CD31
CD45-TER119-CD31-
Ebf2 - GFP
4.65
CD44
CD45-TER119-CD31-CD44- Ebf2+
CD140a
PαS
71.3
CD51
SCA1
CD45-TER119-CD31-CD44-Ebf2-
41.12
B
of PI-
% Ebf2+ Cells
C
of CD45-TER119-CD31-
D
% PαS of Ebf2+ cells
% PαS of Ebf2- cells
Ebf2+
Ebf2-
E
<0.0001
CFU-Fs / 100cells
F
0.0003
SCA1+ SCA1-
G
Skin Ebf2+ cells
negative response (%)
Y = -10.19*X + 79.33
R2 = 0.9300
37,5
Cell dose
H
8 Ebf2+ clones
Osteogenic and Adipogenic (87,5%)
No differentiation
I
Skin Ebf2- PaS cells
Y = -7.542*X + 70.94
R2 = 0.8659
J
7 Ebf2-PαS clones
Osteogenic and Adipogenic (42,86%)
Osteogenic only (14,29%)
No differentiation
K
Ebf2+ clones
Osteogenic
Adipogenic
#1
#2
#3
Ebf2-PαS clones
L
Skin Ebf2+ clone
Population doubling time (days)
Passage
F4
F6
F7
F10
F11
Skin Ebf2-PαS clone
F6

Figure 3

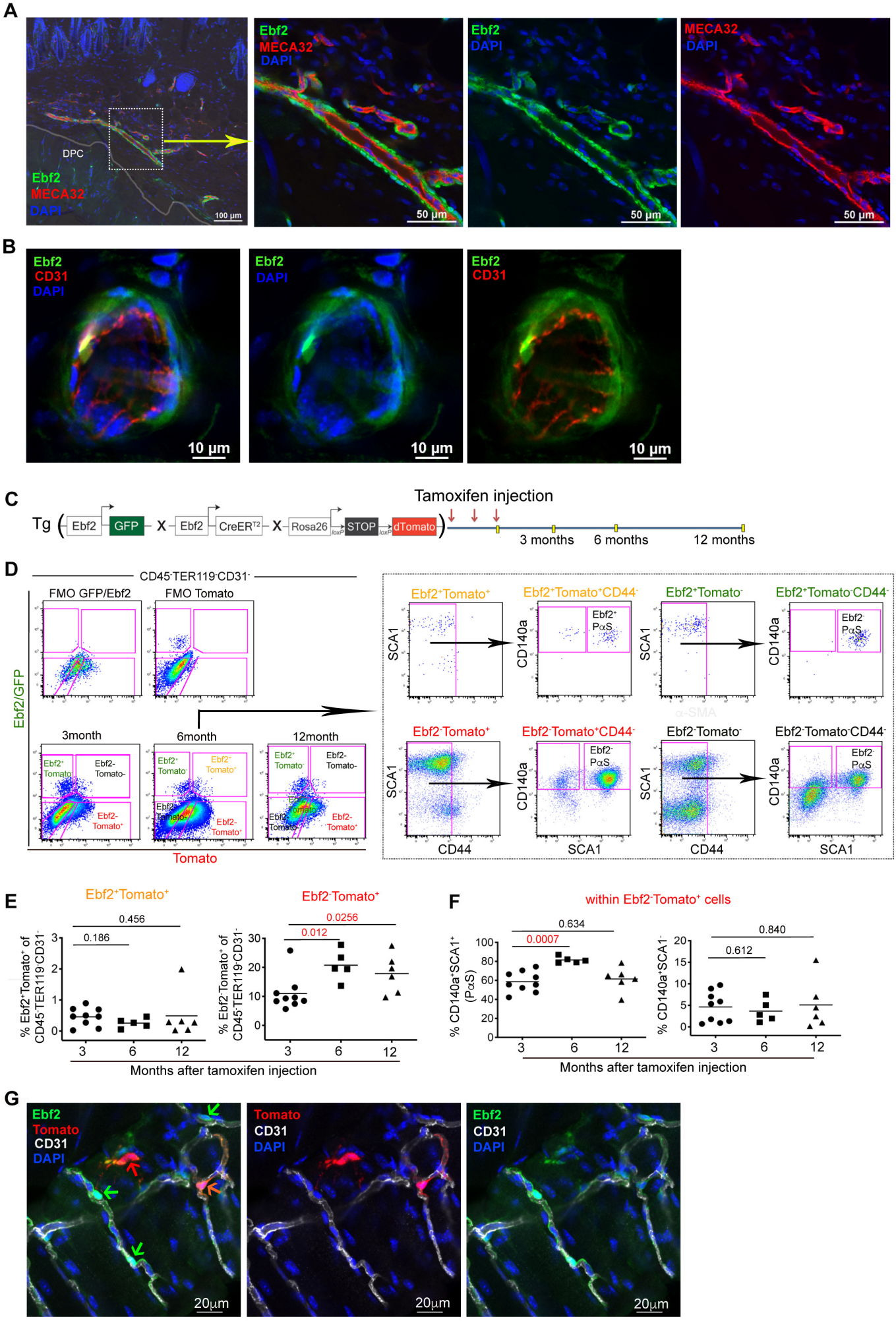
A
DPC
Ebf2
MECA32
DAPI
100 µm
50 µm
B
CD31
10 µm
C
Tg
Ebf2
GFP
X
CreER^{T2}
Rosa26
STOP
dTomato
Tamoxifen injection
3 months
6 months
12 months
D
CD45$^-$TER119$^-$CD31$^-$
FMO GFP/Ebf2
FMO Tomato
Ebf2/GFP
3month
6month
12month
Tomato
Ebf2$^+$Tomato$^+$
Ebf2$^+$Tomato$^+$CD44$^-$
Ebf2$^+$Tomato$^-$
Ebf2$^+$Tomato$^-$CD44$^-$
Ebf2$^-$Tomato$^+$
Ebf2$^-$Tomato$^+$CD44$^-$
Ebf2$^-$Tomato$^-$
Ebf2$^-$Tomato$^-$CD44$^-$
SCA1
CD140a
CD44
PαS
α-SMA
E
Ebf2$^+$Tomato$^+$
Ebf2$^-$Tomato$^+$
% Ebf2$^+$Tomato$^+$ of CD45$^-$TER119$^-$CD31$^-$
% Ebf2$^-$Tomato$^+$ of CD45$^-$TER119$^-$CD31$^-$
0.456
0.186
0.0256
0.012
Months after tamoxifen injection
F
within Ebf2$^-$Tomato$^+$ cells
% CD140a$^+$SCA1$^+$ (PαS)
% CD140a$^+$SCA1$^-$
0.634
0.0007
0.840
0.612
Months after tamoxifen injection
G
Ebf2
Tomato
CD31
DAPI
20µm

Figure 4

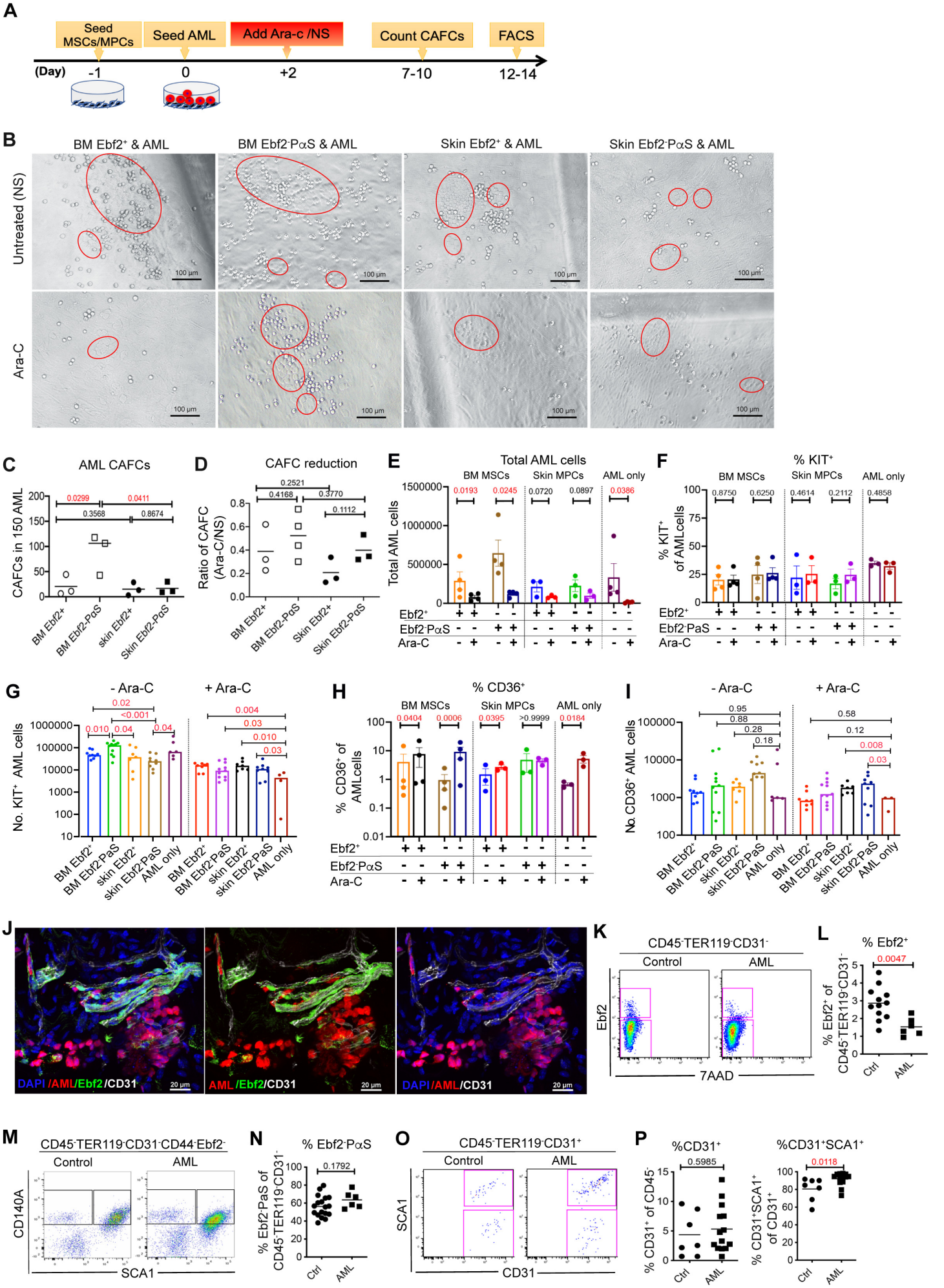
A
Seed MSCs/MPCs
Seed AML
Add Ara-c /NS
Count CAFCs
FACS
(Day)
-1
0
+2
7-10
12-14
B
BM Ebf2+ & AML
BM Ebf2-PαS & AML
Skin Ebf2+ & AML
Skin Ebf2-PαS & AML
Untreated (NS)
Ara-C
100 µm
C
AML CAFCs
CAFCs in 150 AML
0.0299
0.0411
0.3568
0.8674
BM Ebf2+
BM Ebf2-PαS
skin Ebf2+
Skin Ebf2-PαS
D
CAFC reduction
Ratio of CAFC (Ara-C/NS)
0.2521
0.4168
0.3770
0.1112
E
Total AML cells
BM MSCs
Skin MPCs
AML only
Total AML cells
0.0193
0.0245
0.0720
0.0897
0.0386
Ebf2+
Ebf2-PαS
Ara-C
F
% KIT+
% KIT+ of AMLcells
0.8750
0.6250
0.4614
0.2112
0.4858
G
- Ara-C
+ Ara-C
No. KIT+ AML cells
0.02
<0.001
0.010
0.04
0.04
0.004
0.03
0.010
0.03
H
% CD36+
% CD36+ of AMLcells
0.0404
0.0006
0.0395
>0.9999
0.0184
I
No. CD36+ AML cells
0.95
0.88
0.28
0.18
0.58
0.12
0.008
0.03
J
DAPI/AML/Ebf2/CD31
AML/Ebf2/CD31
DAPI/AML/CD31
20 µm
K
CD45-TER119-CD31-
Control
AML
Ebf2
7AAD
L
% Ebf2+
% Ebf2+ of CD45-TER119-CD31-
0.0047
Ctrl
AML
M
CD45-TER119-CD31-CD44-Ebf2-
Control
AML
CD140A
SCA1
N
% Ebf2-PαS
% Ebf2-PaS of CD45-TER119-CD31-
0.1792
Ctrl
AML
O
CD45-TER119-CD31+
Control
AML
SCA1
CD31
P
%CD31+
% CD31+ of CD45-
0.5985
%CD31+SCA1+
% CD31+SCA1+ of CD31+
0.0118
Ctrl
AML

Figure 5

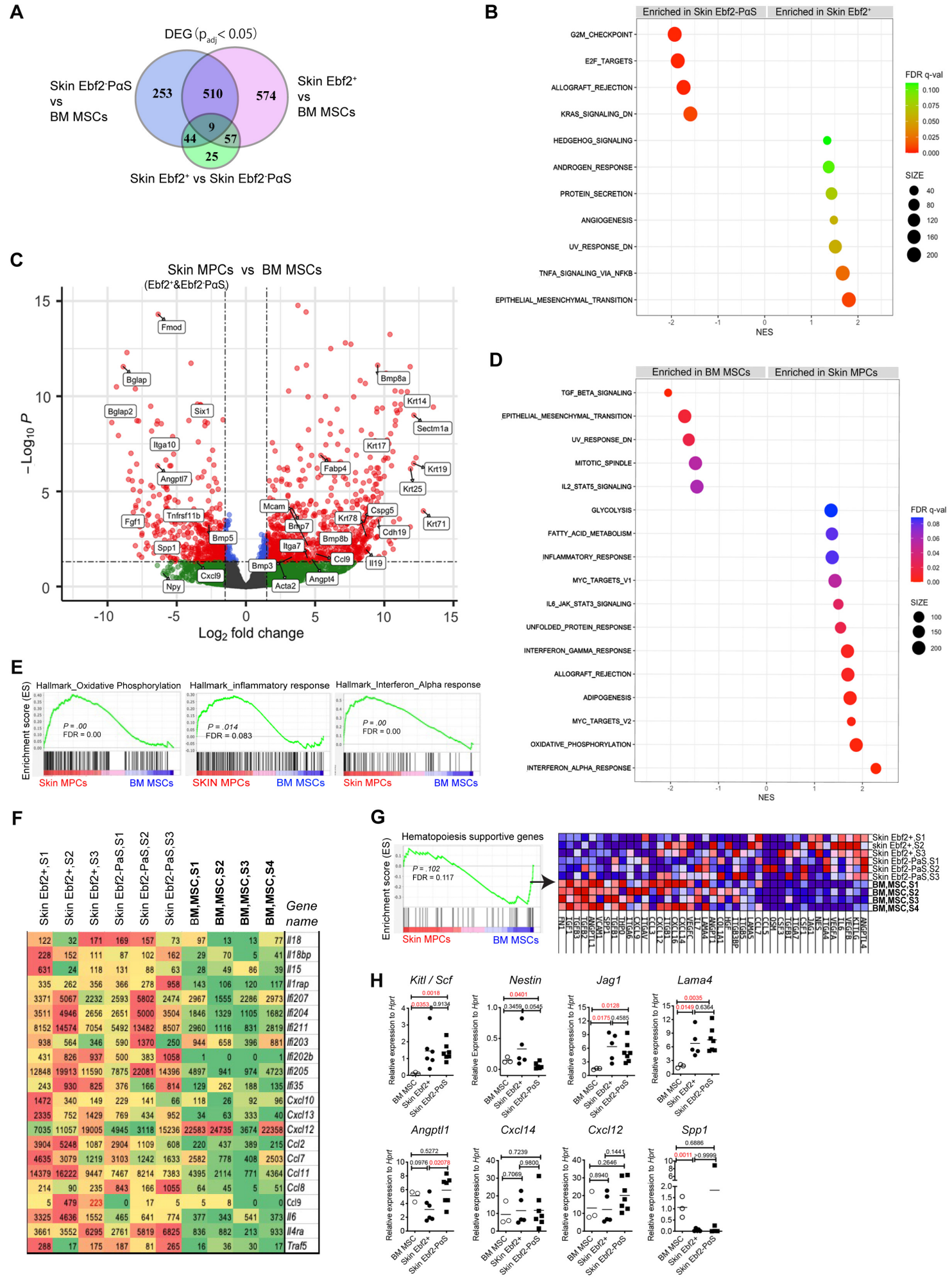
A
DEG (p_{adj} < 0.05)
Skin Ebf2⁻PαS vs BM MSCs
Skin Ebf2⁺ vs BM MSCs
Skin Ebf2⁺ vs Skin Ebf2⁻PαS
253
510
574
9
44
57
25
B
Enriched in Skin Ebf2-PαS
Enriched in Skin Ebf2⁺
G2M_CHECKPOINT
E2F_TARGETS
ALLOGRAFT_REJECTION
KRAS_SIGNALING_DN
HEDGEHOG_SIGNALING
ANDROGEN_RESPONSE
PROTEIN_SECRETION
ANGIOGENESIS
UV_RESPONSE_DN
TNFA_SIGNALING_VIA_NFKB
EPITHELIAL_MESENCHYMAL_TRANSITION
NES
FDR q-val
SIZE
C
Skin MPCs vs BM MSCs
(Ebf2⁺&Ebf2⁻PαS)
−Log10 P
Log2 fold change
Fmod
Bglap
Bglap2
Six1
Itga10
Angptl7
Fgf1
Tnfrsf11b
Bmp5
Spp1
Cxcl9
Npy
Bmp8a
Krt14
Sectm1a
Krt17
Fabp4
Krt19
Krt25
Mcam
Bmp7
Krt78
Cspg5
Krt71
Cdh19
Bmp8b
Itga7
Ccl9
Il19
Bmp3
Angpt4
Acta2
D
Enriched in BM MSCs
Enriched in Skin MPCs
TGF_BETA_SIGNALING
EPITHELIAL_MESENCHYMAL_TRANSITION
UV_RESPONSE_DN
MITOTIC_SPINDLE
IL2_STAT5_SIGNALING
GLYCOLYSIS
FATTY_ACID_METABOLISM
INFLAMMATORY_RESPONSE
MYC_TARGETS_V1
IL6_JAK_STAT3_SIGNALING
UNFOLDED_PROTEIN_RESPONSE
INTERFERON_GAMMA_RESPONSE
ALLOGRAFT_REJECTION
ADIPOGENESIS
MYC_TARGETS_V2
OXIDATIVE_PHOSPHORYLATION
INTERFERON_ALPHA_RESPONSE
NES
FDR q-val
SIZE
E
Hallmark_Oxidative Phosphorylation
Hallmark_inflammatory response
Hallmark_Interferon_Alpha response
Enrichment score (ES)
P = .00
FDR = 0.00
P = .014
FDR = 0.083
P = .00
FDR = 0.00
Skin MPCs
BM MSCs
SKIN MPCs
BM MSCs
Skin MPCs
BM MSCs
F
Skin Ebf2+,S1
Skin Ebf2+,S2
Skin Ebf2+,S3
Skin Ebf2-PaS,S1
Skin Ebf2-PaS,S2
Skin Ebf2-PaS,S3
BM,MSC,S1
BM,MSC,S2
BM,MSC,S3
BM,MSC,S4
Gene name
122 32 171 169 157 73 97 13 13 77 Il18
228 152 111 87 102 162 29 70 5 41 Il18bp
631 24 118 131 88 63 28 49 86 39 Il15
335 262 356 366 278 958 143 106 120 117 Il1rap
3371 5067 2232 2593 5802 2474 2967 1555 2286 2973 Ifi207
3511 4946 2656 2651 5000 3504 1846 1329 1105 1682 Ifi204
8152 14574 7054 5492 13482 8507 2960 1116 831 2819 Ifi211
938 564 346 590 1370 250 944 658 396 881 Ifi203
431 826 937 500 383 1058 1 0 0 1 Ifi202b
12848 19913 11590 7875 22081 14396 4897 941 974 4723 Ifi205
243 930 825 376 166 814 129 262 188 135 Ifi35
1472 340 149 229 141 66 118 26 92 96 Cxcl10
2335 752 1429 769 434 952 34 63 333 40 Cxcl13
7035 11057 19005 4945 3118 15236 22583 24735 3674 22358 Cxcl12
3904 5248 1087 2904 1109 608 220 437 389 215 Ccl2
4635 3079 1219 3103 1242 1633 2582 778 408 2503 Ccl7
14379 16222 9447 7467 8214 7383 4395 2114 771 4364 Ccl11
214 90 235 843 166 1055 64 45 5 51 Ccl8
5 479 223 0 17 5 5 8 0 0 Ccl9
3325 4636 1552 465 641 774 377 343 541 373 Il6
3661 3552 6295 2761 5819 6825 836 882 213 933 Il4ra
288 17 175 187 81 265 16 36 30 17 Traf5
G
Hematopoiesis supportive genes
Enrichment score (ES)
P = .102
FDR = 0.117
Skin MPCs
BM MSCs
Skin Ebf2+,S1
skin Ebf2+,S2
Skin Ebf2+,S3
Skin Ebf2-PaS,S1
Skin Ebf2-PaS,S2
Skin Ebf2-PaS,S3
BM,MSC,S1
BM,MSC,S2
BM,MSC,S3
BM,MSC,S4
FN1 IGF1 TGFB3 HGF EGF1L1 VCAM1 SPP1 TGFB1 THPO TTGA6 CTGAV CTGAV CCL3 CXCL12 ITGB1 CXCL16 VEGFA VEGFC IL7 LAMA4 ANGPT1 COL1A1 HGF38P ITGB5 LAMA5 CCL7 CCL5 OSM IL4 TGFB1 TTGA7 CSF1 JAG1 NES CXCL4 VEGFA IL6 VEGFB KITLG ANGPTL4
H
Kitl / Scf
Nestin
Jag1
Lama4
Angptl1
Cxcl14
Cxcl12
Spp1
Relative expression to Hprt
BM MSC
Skin Ebf2+
Skin Ebf2-PaS

Figure 6

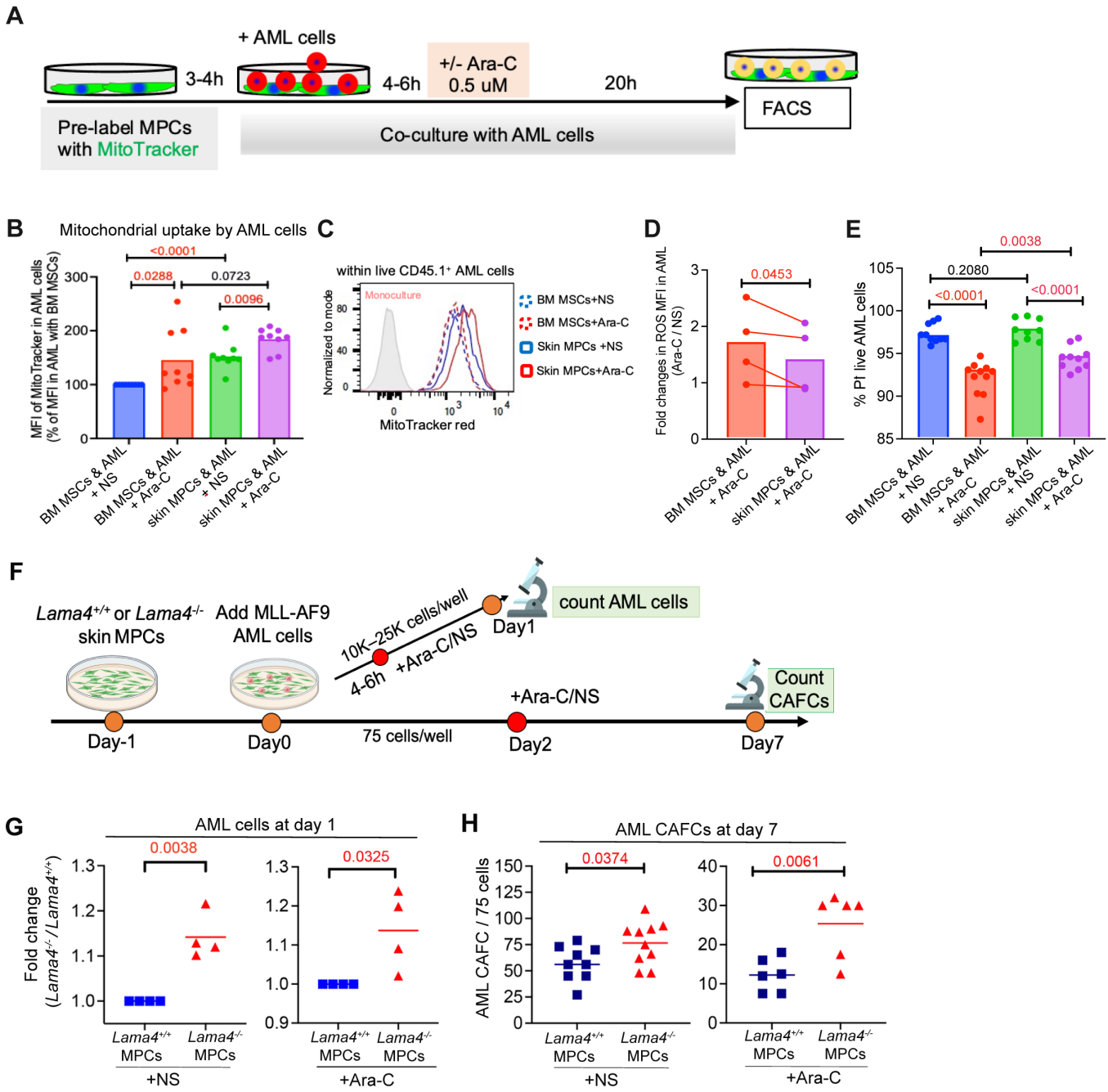
A
+ AML cells
3-4h
4-6h
+/- Ara-C
0.5 uM
20h
FACS
Pre-label MPCs
with MitoTracker
Co-culture with AML cells
B
Mitochondrial uptake by AML cells
MFI of MitoTracker in AML cells
(% of MFI in AML with BM MSCs)
<0.0001
0.0288
0.0723
0.0096
BM MSCs & AML + NS
BM MSCs & AML + Ara-C
skin MPCs & AML + NS
skin MPCs & AML + Ara-C
C
within live CD45.1+ AML cells
Monoculture
Normalized to mode
MitoTracker red
BM MSCs+NS
BM MSCs+Ara-C
Skin MPCs +NS
Skin MPCs+Ara-C
D
Fold changes in ROS MFI in AML
(Ara-C / NS)
0.0453
E
% PI live AML cells
0.0038
0.2080
<0.0001
<0.0001
F
Lama4+/+ or Lama4-/- skin MPCs
Add MLL-AF9 AML cells
10K–25K cells/well
4-6h
+Ara-C/NS
Day1
count AML cells
+Ara-C/NS
Count CAFCs
Day-1
Day0
75 cells/well
Day2
Day7
G
AML cells at day 1
Fold change
(Lama4-/-/Lama4+/+)
0.0038
0.0325
Lama4+/+ MPCs
Lama4-/- MPCs
+NS
+Ara-C
H
AML CAFCs at day 7
AML CAFC / 75 cells
0.0374
0.0061

Figure 7

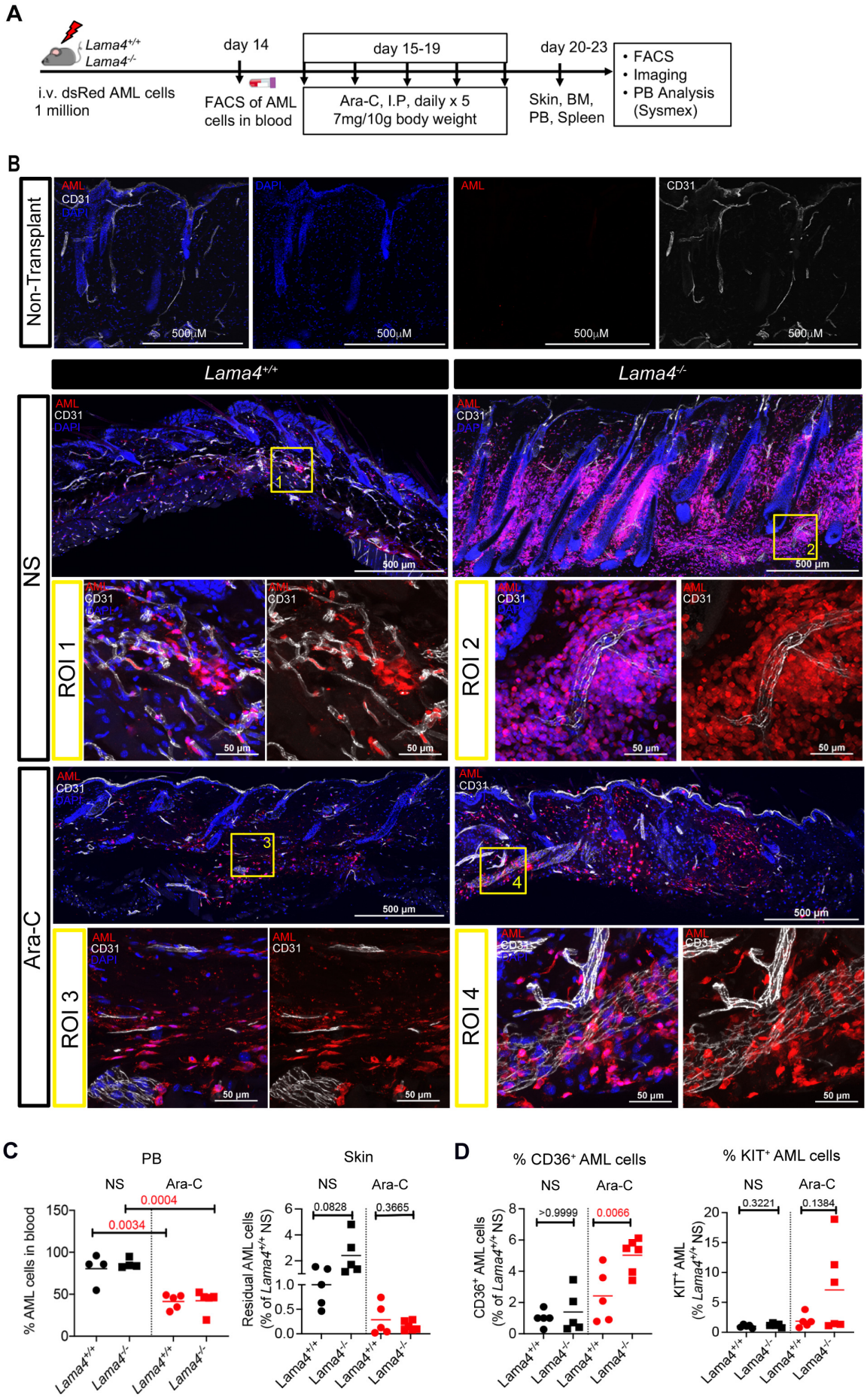
A
Lama4+/+
Lama4-/-
i.v. dsRed AML cells
1 million
day 14
FACS of AML
cells in blood
day 15-19
Ara-C, I.P, daily x 5
7mg/10g body weight
day 20-23
Skin, BM,
PB, Spleen
• FACS
• Imaging
• PB Analysis
(Sysmex)
B
Non-Transplant
AML
CD31
DAPI
500µM
Lama4+/+
Lama4-/-
NS
Ara-C
ROI 1
ROI 2
ROI 3
ROI 4
500 µm
50 µm
C
PB
Skin
NS
Ara-C
0.0004
0.0034
0.0828
0.3665
% AML cells in blood
Residual AML cells
(% of Lama4+/+ NS)
Lama4+/+
Lama4-/-
D
% CD36+ AML cells
% KIT+ AML cells
>0.9999
0.0066
0.3221
0.1384
CD36+ AML cells
(% of Lama4+/+ NS)
KIT+ AML
(% Lama4+/+ NS)